Journal of Geosciences and Geomatics, 2021, Vol. 9, No. 4, 160-176
Available online at http://pubs.sciepub.com/jgg/9/4/1
Published by Science and Education Publishing
DOI:10.12691/jgg-9-4-1

Petrological and Geochemical Characteristics of the Cretaceous Ngaou Boh Anorogenic Complex (Adamawa Plateau, Cameroon Line): Preliminary Constraints

Zénon Itiga[1,*], Benoît Joseph Mbassa[2], Rose Noël Ngo Belnoun[3], Pierre Wotchoko[4], Dieudonné Tchokona Seuwui[5], Sébastien Owona[1], Jacques-Marie Bardintzeff[6], Pierre Wandji[5], Hervé Bellon[7]

[1]Department of Earth Sciences, University of Douala, P.O. Box 24157, Douala, Cameroon
[2]Institute for Geological and Mining Research, Laboratory of Ore mineral Processing, P.O. Box 4110, Yaoundé, Cameroon
[3]Department of Earth Sciences, University of Yaoundé, P.O. Box 812, Yaoundé, Cameroon
[4]Higher Teacher Training College, University of Bamenda I, P.O. Box 39, Yaoundé, Cameroon
[5]Higher Teacher Training College, University of Yaoundé I, P.O. Box 47, Yaoundé, Cameroon
[6]Université Paris-Saclay, Sciences de la Terre, Volcanologie, Planétologie, UMR CNRS, 8148 GEOPS, bât 504, F-91405, Orsay, France
[7]Université européenne de Bretagne, CNRS UMR, 6538 Domaines océaniques, UBO-IUEM, 6 avenue Le Gorgeu, CS 93837, F-29238, Brest cedex 3, France
*Corresponding author: zenonitiga@yahoo.fr

Received July 23, 2021; Revised August 29, 2021; Accepted September 07, 2021

Abstract The Cretaceous Ngaou Boh anorogenic complex (NBAC) located in the far North Adamawa Plateau, the centre domain of the Cameroon Line constitutes a plutonic-volcanic ring association. The whole rock K-Ar datation yields a crystallization age of ca. 74 Ma. Plutonic rocks comprise abundant alkali feldspar granites, scarce clinopyroxene-amphibole gabbros and alkali feldspar syenites. Alkali feldspar granites are leucocratic, coarse to fine-grained; quartz and K-feldspars are the major rock-forming mineral, besides minor oligoclase, biotite and accessory phases as sphene, zircon and opaques. Alkali feldspar syenites are mesocratic coarse-grained, mainly composed of K-feldspars with small amounts of quartz and biotite. Volcanic rocks consist of a basanite-trachyte-rhyolite suite. Basanites contain olivine and diopside phenocrysts and a groundmass essentially composed of plagioclase and titanomagnetite. Biotite-clinopyroxene trachytes and clinopyroxene-amphibole rhyolites have an almost homogeneous modal composition, mainly made up of sanidine and anorthoclase microliths, scarce phenocrysts of quartz, and minor crystals of biotite, clinopyroxene (augite) amphibole (pargasite, sandagaite); Fe-Ti oxides (ilmenite, titanomagnetite) and fibreglass are often isolated in the groundmass. Plutonic rocks are alkaline, weakly metaluminous with some alkali feldspar granites displaying agpaitic or peralkaline feature. Incompatible Trace elements (HFSE and LILE) distribution and chondrite-normalized REE patterns evidence a significant petrogenetic link between clinopyroxene-amphibole gabbros, alkali feldspar syenites and alkali feldspar granites. All the analysed samples are enriched in incompatible elements, indicating melts from spinel and garnet-bearing mantle source close to OIB component. Indeed, the $(Tb/Yb)_N$ ratios of both basanites (2.3-2.5) and clinopyroxene-amphibole gabbros (1.4-1.9) suggest different parental magma sources. Alkali feldspar granites appear as residue of magma differentiation led by crystal fractionation of liquid derived from the partial melting of spinel peridotite mantle. Clinopyroxene-amphibole rhyolites and biotite-clinopyroxene trachytes ($Mg^{\#}$=0.0-15.4) derive through fractional crystallization from basanites ($Mg^{\#}$=64.3-60.1), the most primitive mafic parental melt. Both plutonic rocks and lavas trends evidence a bimodality highlighted by a pronounced "Daly gap".

Keywords: *Ngaou Boh, Cameroon Line, Adamawa Plateau, anorogenic complex, magma differentiation, K/Ar age dating*

Cite This Article: Zénon Itiga, Benoît Joseph Mbassa, Rose Noël Ngo Belnoun, Pierre Wotchoko, Dieudonné Tchokona Seuwui, Sébastien Owona, Jacques-Marie Bardintzeff, Pierre Wandji, and Hervé Bellon, "Petrological and Geochemical Characteristics of the Cretaceous Ngaou Boh Anorogenic Complex (Adamawa Plateau, Cameroon Line): Preliminary Constraints." *Journal of Geosciences and Geomatics*, vol. 9, no. 4 (2021): 160-176. doi: 10.12691/jgg-9-4-1.

1. Introduction

The Cameroon Line (CL) is the major magmatic and tectonic feature in Central Africa underlined by several volcanic bodies most of Cenozoic era following the SSW-NNE direction. The CL extends from the Pagalú Island in the Atlantic Ocean [1] passing through the Cameroonian territory up to Tibesti in Chad, almost more than 1500 km long and 100 km wide. The continental sector of the CL consists of a succession of horsts, plains of collapse or grabens and plutonic-volcanic complexes. The horsts correspond to the major volcanic systems (Mount Cameroon, Mounts Bamenda, Mounts Bambouto, Mount Manengouba, a.s.o.) while the main plains of collapse or grabens are Kumba, Tombel, and Noun [2,3,4]. More than sixty plutonic-volcanic complexes located in the South (e.g. Ntumbaw and Nda Ali) and in the North (e.g. Kokoumi, Tchégui, Mboutou and Golda Zuelva), mainly in the central sector of the CL, notably in the Tikar plain (Pandé, Sabongari and Nana massifs) and the Adamawa Plateau (Mayo Darlé, Hosséré Nigo, Hosséré Guenfalabo and Ngaou Boh) have been identified. However, numerous anorogenic complexes have not yet been studied such as the Ngaou Boh which is the focus of this work. Several previous works from most of those complexes [5-14] evidence discontinuous magmatic sequences with more or less pronounced "Daly gap" i.e. scarce or none intermediate rocks, except the Guenfalabo massif which forms a continuous series. Anorogenic complexes from CL are alkaline, SiO_2-saturated or SiO_2-oversaturated, but some display peralkaline constraints such as the presence of Na-pyroxenes and Na-amphiboles (Pandé, Nda Ali, Kokoumi). Plutonic rocks (granite, syenite, gabbro) constantly predominate on volcanics. The Cenozoic ages of these complexes extend from ca.69 Ma for Guenfalabo [15] to ca.38 Ma for Mboutou and Golda Zuelva [6]. Amongst these ring complexes only Mayo Darlé has a mineralizing potential borne out by the presence of high tin concentration. In this paper we report preliminary petrographical, mineralogical, geochemical and geochronological features relevant to the Ngaou Boh anorogenic complex and discuss sources and magma differentiation.

2. Geology and Regional Background

The NBAC is located within the Gapi graben at the far SSW from the Tchabal Gangdaba volcano [16,17] in the vicinity of the Gapi Stock [18] upon the edge of the Adamawa Plateau (Figure 1). Ngaou Boh is a volcanic-plutonic ring complex (6 km of the longest diameter) rising up to 1986 m above sea level, and characterized by a collapse at its top as a flat-bottomed depression in a shape of caldera. Such structure has been identified in the Nda Ali plutonic-volcanic ring complex [9]. The basement of the NBAC is composed of Pan-African anatexite and migmatite [19].

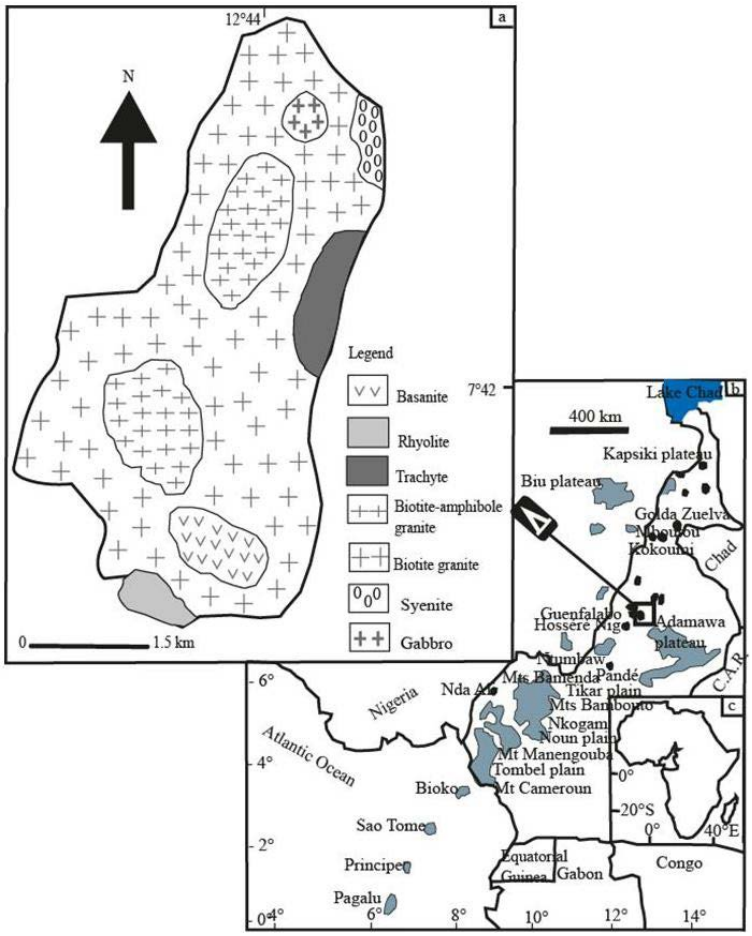

Figure 1. (a) Geological sketch map of the NBAC; (b) location of NBAC in the CL and (c) location of Cameroon in Africa. Main volcanic bodies are in ash-grey and some anorogenic plutons in black. C.A.R: Central African Republic

Field observations reveal a succession of plutonic and volcanic rocks. The lithology of the NBAC includes from the bottom to the summit of 1986 m: clinopyroxene-amphibole gabbro, alkali feldspar syenite, biotite-clinopyroxene trachyte, alkali feldspar granite and basanite. But, this petrographic sequence is not regular everywhere because of the absence or scarcity of some of the above-mentioned rock types.

Plutonic rocks crop out either as chaotic metric boulders in the shape of variable bowls or as little intrusion shape recalling curved structures of ring dyke. Clinopyroxene-amphibole gabbros and alkali feldspar syenites constitute weathered and destabilized dykes, scattered in blocks or bowls of several meters size. Leucocratic alkali feldspar granites and ash-gray alkali feldspar granites outcrop in the centre at altitude 1730 m as blocks or domes. At a hundred meters from the southeast inside edge, outcrops a ring dyke of basanite surrounded by porphyroid alkali feldspar granite.

The lava flows occurring at altitude 1680 m have been essentially fissural. Thus, towards the summit on the SE flank, there is a thin basanitic outpouring, while radial veins and rings of biotite-clinopyroxene trachyte and clinopyroxene-amphibole rhyolite curve the outer edges of the ESE and SW sides. This volcanism is likely the last magmatic event during the emplacement of NBAC as evidenced by the orientation of most volcanic veins (N100 for basanites, N35 and N105 for trachyte and rhyolite) which are parallel to the fracturing of the whole massif.

Hosséré Nigo and Hosséré Guenfalabo, two other anorogenic ring complexes in the vicinity of Ngaou Boh are E-W oriented. They widely consist of plutonic silica-under or oversaturated alkaline rocks. Hosséré Nigo (7°50 N, 12°39 E, 1750 m a.s.l.) is mainly made up of gabbro, monzonite and syenite of 65.0 ± 0.8 Ma [14] whereas the Guenfalabo complex (7°40 N, 12°25 E, 1650 m a.s.l.) yields two complete suites of volcanic rocks (basanite-rhyolite) and plutonic rocks (gabbro-granite) dated ca.68.8±1.7 Ma [15].

3. Results

3.1. K-Ar Age Dating

Whole rock $^{40}K/Ar^{40}$ dating were performed at the *Laboratoire de Géochronologie, Université européenne de Bretagne*, at Brest, France, following the analytical procedure detailed by [20]. Constant values of [21] have been used for age calculations. Uncertainties given at 1σ have been calculated following [22].

The anorogenic complexes previously dated in CL through Ar/Ar, K/Ar and Rb/Sr methods all yield Tertiary ages (ca. 70-39 Ma) except the Mayo Darlé complex (ca. 73-54 Ma) [5].

Two ages dating using whole rock $^{40}K/^{40}Ar$ method provided ca.74.21 ± 1.71 Ma and ca. 72.42 ± 1.67 Ma with the mean of 73. 31 ± 1.71 Ma (Late Campanian) indicating the age of crystallization of coarse-grained alkali feldspar granite from the NBAC (Table 1). These ages are older compared to those of the neighbouring Hosséré Nigo (ca. 65.3 ± 0.8 Ma; [14] and Hosséré Guenfalabo (ca. 68.8 ± 1.7 Ma [15] obtained using respectively phlogopite $^{40}Ar/^{39}Ar$ and whole rock $^{40}K/^{39}Ar$ dating. According to the aforementioned ages, the Ngaou Boh should so far be considered as the oldest anorogenic complex dated in Cameroon, since most ages available range between ca. 60-70 Ma.

3.2. Petrography and Mineralogy

Micropobe analyses of the representative samples of petrographic types were performed at the *Université Paris-Sorbonne*, France, using a Cameca SX100 Microprobe (15 kV, 10 nA). Kα lines were used. International geostandards were used: diopside for Si, Ca and Mg, Fe_2O_3 for Fe, $MnTiO_3$ for Ti and Mn, Cr_2O_3 for Cr, albite for Na, orthoclase for K and Al. Counting times were 10s for both peaks and background, with a 5-µm defocused beam.

3.2.1. Volcanic Rocks

NBAC volcanic rocks are composed of a little mafic unit (basanites) and mainly felsic unit (trachytes, rhyolites).

Basanites are melanocratic and aphanitic small blocks issued from destabilized dyke. These rocks display aphyric microlitic and fluid texture (Figure 2a). Phenocrysts (11.5 vol. %; > 0.35 mm) concern clinopyroxene whereas microphenocrysts (< 0.35 mm) and microlites (< 0.035 mm) are composed of clinopyroxene, olivine and plagioclase. Clinopyroxene phenocrysts have a diopside composition ($En_{35-41}Wo_{46-50}Fs_{13-15}$) [23] (Table 2). Some sections sometimes cluster together into rosettes or aggregates. Olivine (chrisotile) microphenocrysts are frequently embayed with Fe-Ti oxides. The ferrotitanium oxides generally form anhedral titanomagnetite microphenocrysts (mol % usp: 0.61-0.58; Ilm: 0.39-0.42 mol %) (Table 3) scattered within the groundmass (88.5 vol. %). Traces of skeletal nepheline microphenocrysts often occur. Plagioclase microlites (labradorite-andesine, An_{54-39}) (Table 4), the most abundant mineral phase of the groundmass, are locally oriented.

Biotite-clinopyroxene trachytes outcrop as decametric whitish or ash-gray coloured blocks. They have a porphyritic microlitic texture (Figure 2b and c). Phenocryst phases (15.8 vol. %) are composed of rods, chopsticks or subhedral anorthoclases. But the most developed phenocrysts (0.9 × 0.9 mm) are always anhedral. Biotite microphenocrysts (0.25 x 0.2 mm), most often altered, occur as lamellas often including sanidine microlites. Primary Fe-Ti oxides form granular microphenocrysts sparse in the groundmass. This groundmass (84.2 vol. %) is essentially made up of sanidine microlites and slight reddish-brownish glassy matrix. Within the groundmass, augite constitutes some interstitial anhedral microcrystals slipped in between sanidine microlites.

Clinopyroxene-amphibole rhyolites, gray-coloured, occur at the foot of the Ngaou Boh SW slope as a dyke. The porphyritic texture is marked by the irregular appearance of whitish millimetric alkali feldspars phenocrysts. This rhyolite is atypical due to the abundant spherulitic and radiating alkaline feldspar rods. The phenocrysts (16.5 vol. %) are mainly sanidine, anorthoclase, quartz and amphibole (Figure 2d). Sanidine

is the most abundant mineral phase, present either as elongated phenocrysts or medium sized laths. Anorthoclase exceptionally constitutes thickset chopsticks and prisms. Quartz euhedral phenocrysts are the most developed mineral phase (up to 1.20 x 1.36 mm). Amphibole phenocrysts generally constitute skeletal crystals often replaced by chlorite in the core and oxide at the border. The groundmass (79 vol. %) includes in addition of sanidine and anorthoclase microlites, rods and strips plagioclase altered into sericite, little amount of augite, microlites, acicular or anhedral Fe-Ti oxides, and quite abundant light brown glass (4.5 vol. %). The latter also display sometimes elongated fibres commonly arranged into spherulites.

Table 1. Whole rock $^{40}K/^{40}Ar$ age dating of coarse-grained alkali feldspar granite from NBAC

Sample	Analysis	Age (Ma)	^{36}Ar Exp.(10^{-9} cm^3)	$^{40}Ar^*$ (%)	$^{40}Ar^*/g(10^{-7}cm^3)$	K_2O (%)
I34	B6663-6	72.42 ± 1.67	2.231	94.4	110.800	4.65
I34	B6677-4	74.21 ± 1.71	1.042	90.5	113.600	4.65
Mean		73.31 ± 1.71				

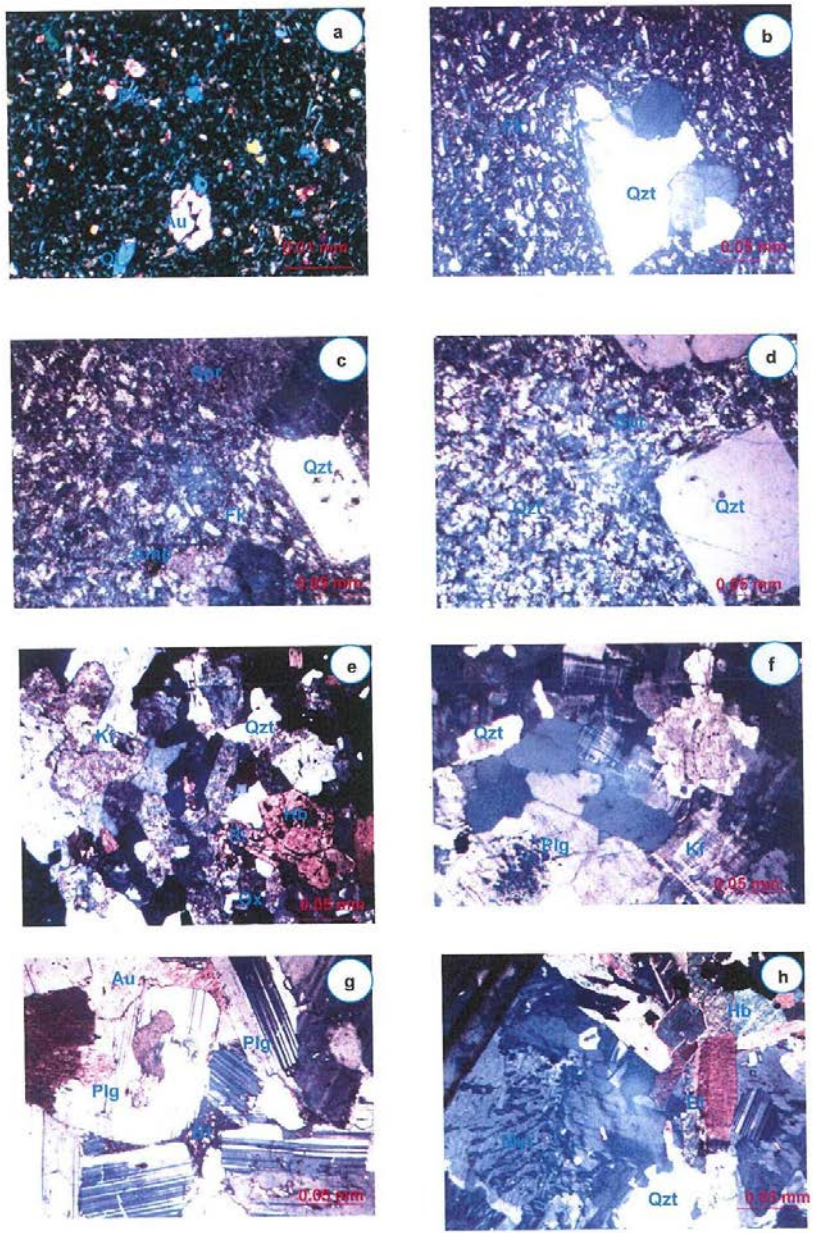

Figure 2. Photomicrographs of representative NBAC plutonic and volcanic rocks (a) Microlithic porphyritic texture in basanite HG5. The microphenocrysts of olivine and augite are embedded in a groundmass of microlites of plagioclase, Fe-Ti oxide and glass. (b) Porphyritic microlitic texture with a fluid tendency in a trachyte (sample TG20). In the center, sanidine and anorthoclase microlites encompass a quartz porphyrocrystal. (c) Trachyte (sample I21) more or less altered. (d) Equigranular and porphyritic microlitic texture with corroded euhedral quartz phenocryst in rhyolite I33. Microlites of sanidine and anorthoclase, and Fe-Ti oxide granules essentially compose the fined matrix. (e, f) Fine to coarse-grained equigranular textures in alkali feldspar granites (I30, I35) showing sometimes altered alkaline feldspars. (g) Coarse-grained and intersertal texture in clinopyroxene-amphibole gabbro TG23. Pseudomorphose of augite crystals into serpentine or uralite and plagioclase minerals in the process of being sericitized. (h) Heterogranular coarse-grained texture in a syenite (I38). Alkaline feldspars are mainly perthitic and myrmekitic. Au: augite; Bt: biotite; Fk: alkaline feldspar; Hb: hornblende; Ol: olivine; Ox: Fe-Ti oxide; Myr: myrmekite; Spr: spherulite; Qzt: quartz

3.2.2. Plutonic Rocks

The NBAC plutonic rocks are made up of leucocratic granite, ash-gray amphibole ± biotite granite, syenite and gabbro.

The NBAC leucocratic alkali feldspar granites are whitish, heterogranular and coarse-grained rocks mainly consist of alkali feldspar, quartz, plagioclase, green hornblende, biotite and Fe-Ti oxides (Figure 2e). Alkali feldspar (41 vol. %), the predominant mineral, rarely exhibits the Carlsbad twin and consists of orthoclase and microcline. Plagioclase appears as euhedral megaphenocrysts (4-6 mm) and microphenocrysts (0.8 x 0.5 mm). The rims of phenocrysts are usually indented or altered into sericite or epidote while the microphenocrysts are fully saussuritized. Compositions range from oligoclase ($Or_{7-3}Ab_{85-76}An_{19-9}$) to andesine ($Or_4Ab_{70}An_{26}$) (Table 4). Quartz (25 vol. %) crystallized as interstitial anhedral microcrystals. Biotite (3.33 vol. %) appears as greenish or brownish platelets more or less chloritized or oxidized. Biotite phenocrysts always enclose apatite and zircon, whilst microphenocrysts are sometimes included into alkali feldspar. The oxides (2.33 vol. %) are secondary minerals pseudomorphous after hornblende and biotite. They are chemically composed of titanomagnetite (mol % Ilm: 0.97-0.93) (Table 3). Amphiboles (1.66 vol. %) are green hornblende euhedral crystals of various shapes and sizes (chopsticks, needles and tabular) often altered into opaque or chlorite. Chemically, they are sadanagaite (Figure 3; Table 5). The accessory mineral phases (2.12 vol. %) are made up of calcite, zircon and apatite, which are usually included either into biotite crystals or in plagioclase and hornblende (zircon only).

The ash-gray amphibole ± biotite granites are generally exposed as a dome in the innermost part of the NBAC. They locally constitute enclaves (≤ 30 cm size) within leucocratic granite and syenite. Quartz (30 vol. %) occupies the interstitial spaces, where it forms anhedral late microcrysts. Scarce laths and large euhedral crystals of plagioclase (15-20 vol. %) are clustered with biotite minerals. Biotite lamellas (3.3 vol. %) are moderate chloritized or oxidized. The phenocrysts locally enclose apatite and zircon while the smallest crystals are included in alkali feldspar ($Or_{89-63}Ab_{11-37}$). Green hornblende (1.66 vol. %) constitutes euhedral microcrysts of various shapes (chopsticks, needles and platelets) frequently twinned. The pseudomorphic replacement of biotite by chlorite is common; additionally, biotite usually encloses quartz and plagioclase crystals. Opaque minerals (2.3 vol. %) are mostly secondary minerals, resulting from the alteration of biotite and green hornblende. Their chemical composition corresponds to ilmenite (mol % Ilm: 0.93-0.97). Zircon occurs as elongated prisms or granules generally included into biotite (Figure 2e).

The Ngaou Boh alkali feldspar syenite mainly outcrops as metre-sized boulders in the outer flanks, eastern and inner western sides. At the NW and SW flanks syenite occurs as a “ridge”. In general, this rock type is little fresh. In some places, the outcrops present tabular-shaped crystals of feldspar of several centimetres (2.5 cm long and 1.5 cm wide) (Figure 2h). Its coarse grained texture essentially consists of porphyrocrysts of orthoclase (Or_{70} Ab_{30}) (70 vol. %) and medium grains of perthites ($Or_{51-45}Ab_{48-53}$). Rare subeuhedral amphibole phenocrysts (pargasite and sadanagaite) (Table 5; Figure 3) are found in that rock. The biotite flakes are surrounded by quartz and feldspar while millimetric quartz crystals (<10 vol. %) are most scattered.

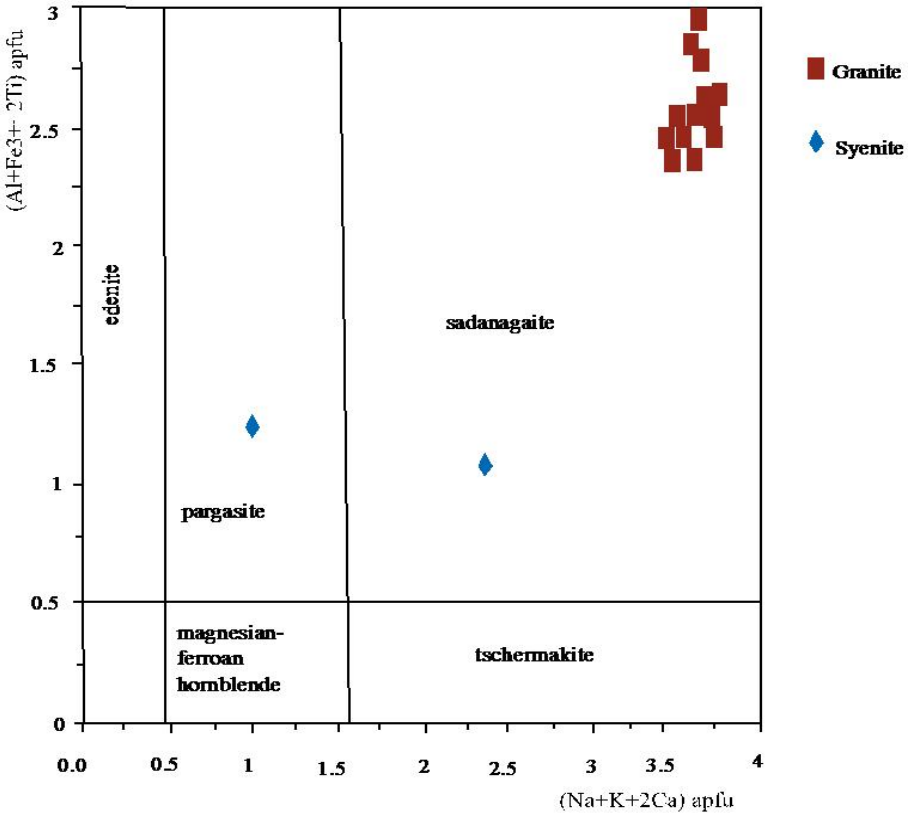

Figure 3. Classification diagram for the NBAC amphibole from [24]

Table 2. Representative electron microprobe analyses of clinopyroxene. Structural formulas calculated on the basis of 4 cations and 6 oxygen anions

Sample	Basanite HG5						Gabbro TG24							
Analysis	1	2	4	5	7	9	10	12	21	117	123	124	125	126
SiO_2	45.05	49.26	44.17	45.03	44.65	45.02	43.59	44.90	50.56	50.54	52.55	52.30	52.02	49.84
TiO_2	4.18	2.32	4.48	3.79	3.46	3.39	4.76	3.19	1.23	0.34	0.40	0.53	0.49	0.05
Al_2O_3	7.26	4.43	8.79	7.32	8.04	6.68	9.09	8.00	3.09	4.53	3.57	3.35	3.41	4.80
Cr_2O_3	0.06	0.00	0.17	0.01	0.23	0.01	0.01	0.24	0.18	0.12	0.11	0.08	0.19	0.03
FeO	8.12	8.33	8.24	8.24	8.71	7.57	8.23	8.25	7.56	18.27	11.87	12.89	13.08	19.95
MnO	0.17	0.20	0.04	0.14	0.12	0.12	0.12	0.08	0.16	0.47	0.27	0.20	0.17	0.50
NiO	0.02	0.05	0.04	0.02	0.05	0.01	0.03	0.00	0.01	0.00	0.03	0.05	0.00	0.03
MgO	12.17	13.30	11.70	12.15	11.77	12.03	11.18	11.87	14.17	10.72	14.77	14.40	14.21	10.51
CaO	22.18	22.18	22.38	22.33	22.72	23.16	22.05	22.37	22.32	10.20	12.52	12.03	12.00	10.09
Na_2O	0.67	0.71	0.80	0.72	0.67	0.75	0.70	0.74	0.62	0.47	0.35	0.25	0.20	0.46
K_2O	0.07	0.06	0.01	0.06	0.01	0.07	0.03	0.03	0.00	0.03	0.02	0.04	0.04	0.05
Total	99.96	100.83	100.82	99.81	100.41	98.82	99.80	99.66	99.91	95.69	96.46	96.11	95.81	96.30
Si	1.70	1.83	1.66	1.70	1.69	1.72	1.65	1.70	1.89	1.98	1.99	2.00	2.00	1.96
Al^{4+}	0.30	0.17	0.34	0.30	0.31	0.28	0.35	0.30	0.11	0.02	0.01	0.00	0.00	0.04
Al^{6+}	0.02	0.03	0.05	0.03	0.04	0.02	0.06	0.06	0.02	0.19	0.15	0.15	0.15	0.19
Cr	0.00	0.00	0.01	0.00	0.01	0.00	0.00	0.01	0.01	0.00	0.00	0.00	0.01	0.00
Ti	0.12	0.06	0.13	0.11	0.10	0.10	0.14	0.09	0.03	0.01	0.01	0.02	0.01	0.00
Fe	0.26	0.26	0.26	0.26	0.27	0.24	0.26	0.26	0.24	0.60	0.38	0.41	0.42	0.66
Mn	0.01	0.01	0.00	0.00	0.00	0.00	0.00	0.00	0.01	0.02	0.01	0.01	0.01	0.02
Ni	0.00	0.00	0.00	0.00	0.00	0.00	0.00	0.00	0.00	0.00	0.00	0.00	0.00	0.00
Mg	0.69	0.74	0.65	0.69	0.66	0.69	0.63	0.67	0.79	0.63	0.84	0.82	0.81	0.62
Ca	0.90	0.88	0.90	0.91	0.92	0.95	0.89	0.91	0.89	0.43	0.51	0.49	0.49	0.43
Na	0.05	0.05	0.06	0.05	0.05	0.06	0.05	0.05	0.04	0.04	0.03	0.02	0.01	0.03
K	0.00	0.00	0.00	0.00	0.00	0.00	0.00	0.00	0.00	0.00	0.00	0.00	0.00	0.00
Sum	4.04	4.03	4.05	4.05	4.06	4.06	4.04	4.05	4.03	3.92	3.93	3.92	3.92	3.94
X_{Mg}	0.73	0.74	0.72	0.72	0.71	0.74	0.71	0.72	0.77	0.51	0.69	0.67	0.66	0.48
SumOx	2.27	2.23	2.25	2.27	2.27	2.30	2.28	2.28	2.24	2.36	2.28	2.30	2.31	2.37
Al^{tot}	0.32	0.19	0.39	0.33	0.36	0.30	0.41	0.36	0.14	0.21	0.16	0.15	0.15	0.22
Number_Ox	6.00	6.00	6.00	6.00	6.00	6.00	6.00	6.00	6.00	6.00	6.00	6.00	6.00	6.00
Fs	14.21	14.07	14.31	14.28	14.99	13.10	14.78	14.00	12.55	36.82	22.28	24.15	24.56	39.25
Wo	48.64	46.85	49.59	48.78	49.40	50.46	50.00	50.00	46.45	25.67	29.43	28.45	28.50	24.80
En	37.15	39.08	36.10	36.94	35.61	36.45	35.22	36.00	41.00	37.51	48.29	47.40	46.94	35.95

Table 3. Representative electron microprobe analyses of Fe-Ti oxides. Structural formulas calculated on the basis of 3 cations and 4 oxygen anions for ulvöspinel-magnetite solid solutions and on the basis of 2 cations and 3 oxygen anions for ilmenite-hematite solid solutions. Usp: ulvöspinel; Mgt: magnetite; Ilm: ilmenite; Hem: hematite

Rock	Basanite				Granite					
Sample	HG5				I30	I32				
Type	Usp-Mgt	Usp-Mgt	Usp-Mgt	Usp-Mgt	Ilm-Hem	Ilm-Hem	Ilm-Hem	Ilm-Hem	Ilm-Hem	Ilm-Hem
Analysis	11	15	16	19	107	63	71	73	74	72
SiO_2	0.04	0.14	0.06	0.05	0.09	0.04	0.16	0.13	0.07	17.49
TiO_2	22.47	23.47	23.64	23.21	47.79	48.65	48.20	49.31	49.00	35.61
Al_2O_3	2.28	2.73	2.84	3.09	0.05	0.00	0.02	0.02	0.03	7.02
Cr_2O_3	0.41	0.41	0.42	0.46	0.05	0.06	0.02	0.13	0.05	0.16
FeO_t	75.32	71.19	73.24	73.17	46.26	42.82	43.92	42.65	43.39	31.99
MnO	0.98	0.86	0.86	0.80	3.35	3.91	3.46	3.88	4.36	2.67
MgO	1.94	3.36	3.45	3.76	0.03	0.04	0.06	0.00	0.00	0.03
CaO	0.10	0.15	0.12	0.16	0.06	0.07	0.04	0.27	0.01	0.17
Na_2O	0.12	0.07	0.05	0.00	0.00	0.00	0.00	0.00	0.00	0.00
K_2O	0.02	0.08	0.06	0.03	0.00	0.00	0.00	0.00	0.00	0.00
NiO	0.09	0.14	0.05	0.09	0.00	0.00	0.00	0.00	0.00	0.01
Total	103.77	102.63	104.79	104.83	97.68	95.59	95.86	96.39	96.91	95.13
Si	0.00	0.00	0.00	0.00	0.00	0.00	0.00	0.00	0.00	0.43
Ti	0.58	0.61	0.60	0.59	0.92	0.96	0.95	0.97	0.96	0.65
Al	0.09	0.11	0.11	0.12	0.00	0.00	0.00	0.00	0.00	0.20
Fe^{+3}	0.72	0.65	0.67	0.69	0.14	0.07	0.09	0.05	0.08	-0.37
Cr	0.01	0.01	0.01	0.01	0.00	0.00	0.00	0.00	0.00	0.00
Fe^{+2}	1.45	1.41	1.40	1.37	0.85	0.87	0.87	0.88	0.86	1.02
Mn	0.03	0.03	0.02	0.02	0.07	0.09	0.08	0.09	0.10	0.06
Mg	0.10	0.17	0.17	0.19	0.00	0.00	0.00	0.00	0.00	0.00
Ca	0.00	0.01	0.00	0.01	0.00	0.00	0.00	0.01	0.00	0.00
Na	0.01	0.00	0.00	0.00	0.00	0.00	0.00	0.00	0.00	0.00
Total	3.01	3.01	3.00	3.00	2.00	2.00	2.00	2.00	2.00	2.00
Fe_2O_3 wt. %	27.82	24.87	26.33	27.12	7.43	3.47	4.48	2.70	4.07	-19.98
FeO wt. %	50.28	48.82	49.55	48.77	39.57	39.70	39.88	40.22	39.73	49.97
Total	104.70	106.10	107.00	107.10	98.40	95.90	96.30	96.50	97.30	93.00
Number Ox onion	4	4	4	4	3	3	3	3	3	3
Usp mole %	0.58	0.60	0.59	0.61						
Mgt mole%	0.42	0.40	0.41	0.39						
Ilm mole %					0.93	0.96	0.96	0.97	0.96	0.95
Hem mole%					0.07	0.04	0.04	0.03	0.04	0.05

Table 4. Representative electron microprobe analyses of feldspars. Structural formulas calculated on the basis of 5 cations and 8 oxygen anions

Rock type	Basanite				Gabbro				Granite										
Sample	HG5				TG24				I30						I32		I34		
Analysis	3	6	13	14	118	119	120	122	114	117	121	123	124	125	81	83	109	110	114
SiO_2	53.26	55.16	53.05	55.06	51.21	51.40	51.22	50.23	64.46	63.51	64.19	61.4	63.18	65.82	64.23	65.27	66.38	65.83	68.26
Al_2O_3	28.23	25.99	29.47	28.30	30.95	30.93	31.16	31.38	21.13	22.04	20.89	23.75	22.65	20.52	18.34	18.69	16.92	18.67	16.58
FeOt	0.36	0.67	0.69	0.64	0.16	0.17	0.18	0.28	0.04	0.06	0.16	0.34	0.07	0.09	0.19	0.12	0.69	0.42	0.86
CaO	10.85	8.40	11.27	9.52	13.20	13.29	13.35	13.86	2.68	3.55	2.01	5.39	3.81	1.80	0.05	0.15	0.00	0.00	0.07
Na_2O	5.20	5.39	5.11	6.09	3.67	3.67	3.72	3.20	9.93	8.96	9.88	8.16	8.40	9.77	1.21	4.11	3.01	6.53	4.91
K_2O	0.49	2.81	0.39	0.46	0.10	0.21	0.13	0.09	0.59	1.21	1.19	0.77	0.90	1.17	14.90	10.94	10.77	8.23	7.93
BaO	0.00	0.23	0.34	0.14	0.00	0.00	0.00	0.00	0.38	0.45	0.05	0.90	0.00	0.12	0	0	0.06	0.00	0.09
Total	98.40	98.66	100.30	100.21	99.29	99.74	99.76	99.02	99.21	99.78	98.37	100.71	99.01	99.29	98.94	99.30	97.82	99.68	98.70
A	2.75	2.71	2.70	2.69	2.75	2.74	2.74	2.77	2.68	2.68	2.70	2.67	2.68	2.67	2.79	2.74	2.82	2.70	2.77
Si	2.44	2.49	2.39	2.46	2.34	2.34	2.33	2.31	2.87	2.83	2.88	2.73	2.82	2.92	2.99	2.98	3.12	2.95	3.15
Al	1.52	1.38	1.56	1.49	1.67	1.66	1.67	1.70	1.11	1.16	1.11	1.25	1.19	1.07	1.01	1.01	0.94	0.99	0.90
Fe	0.01	0.03	0.03	0.02	0.01	0.01	0.01	0.01	0.00	0.00	0.01	0.01	0.00	0.00	0.01	0.00	0.03	0.02	0.03
Ca	0.53	0.41	0.54	0.46	0.65	0.65	0.65	0.68	0.13	0.17	0.10	0.26	0.18	0.09	0.00	0.01	0.00	0.00	0.00
Na	0.46	0.47	0.45	0.53	0.33	0.32	0.33	0.29	0.86	0.77	0.86	0.70	0.73	0.84	0.11	0.36	0.27	0.57	0.44
K	0.03	0.16	0.02	0.03	0.01	0.01	0.01	0.01	0.03	0.07	0.07	0.04	0.05	0.07	0.88	0.64	0.64	0.47	0.47
Ba	0.00	0.00	0.01	0.00	0.00	0.00	0.00	0.00	0.01	0.01	0.00	0.02	-	0.00	0.00	0.00	0.00	0.00	0.00
Total	5.00	5.00	5.00	5.00	5.00	5.00	5.00	5.00	5.02	5.01	5.03	5.01	4.97	5.00	5.00	5.00	5.00	5.00	5.00
Or	2.82	15.56	2.22	2.59	0.59	1.22	0.75	0.56	3.29	6.79	6.65	4.35	5.33	6.67	88.76	63.21	70.18	45.33	51.33
Ab	45.15	45.37	44.06	52.28	33.30	32.90	33.27	29.31	84.16	76.47	83.92	70.1	75.7	84.71	10.97	36.06	29.82	54.67	48.27
An	52.03	39.07	53.72	45.13	66.11	65.88	65.99	70.13	12.55	16.74	9.43	25.57	18.97	8.62	0.27	0.73	0.00	0.00	0.40

Table 5. Representative electron microprobe analyses of amphibole. Structural formulas calculated on the basis of 13 cations eCNK (except Ca, Na and K) and 23 oxygen anions

Rock type	Granite													
Sample	I30			I32									I37	
Analysis	105	112	120	66	67	69	70	75	76	77	79	84	111	115
SiO_2	42.71	42.53	42.92	45.09	43.46	43.77	44.18	43.66	44.06	44.39	43.37	44.40	46.90	46.79
TiO_2	2.13	1.98	1.83	1.58	1.98	1.71	1.75	2.14	1.89	1.63	2.15	1.52	1.42	1.49
Al_2O_3	7.28	6.82	6.95	5.79	6.74	6.77	6.42	6.84	6.64	6.09	6.95	5.78	1.22	1.40
Fe_2O_3	10.20	10.02	9.60	8.56	7.80	7.40	7.01	7.09	7.91	8.27	7.35	9.02	4.18	5.08
FeO	16.41	16.28	17.16	17.41	17.40	18.02	17.62	18.25	17.61	17.16	18.08	17.55	30.46	30.11
MnO	0.85	0.75	0.70	0.42	0.51	0.57	0.46	0.57	0.53	0.61	0.50	0.55	1.44	1.67
MgO	6.96	7.01	6.68	7.36	7.31	7.02	7.31	6.86	7.01	7.29	6.96	6.90	0.32	0.34
CaO	9.81	9.59	9.91	9.66	9.95	9.97	9.63	9.79	9.55	9.73	9.71	9.44	4.30	4.62
Na_2O	2.18	2.23	1.94	2.05	2.14	2.12	2.24	2.18	2.27	2.05	2.35	2.18	5.77	5.71
K_2O	0.97	0.94	0.92	0.73	0.84	0.86	0.84	0.87	0.78	0.74	0.89	0.74	1.34	1.21
Total	99.50	98.15	98.61	98.63	98.18	98.29	97.68	98.35	98.24	97.94	98.30	98.06	97.30	98.42
Si	6.50	6.56	6.59	6.86	6.67	6.72	6.79	6.70	6.75	6.81	6.66	6.83	7.65	7.56
Al^{IV}	1.31	1.24	1.26	1.04	1.22	1.23	1.16	1.24	1.20	1.10	1.26	1.05	0.23	0.27
Al^{VI}	0.00	0.00	0.00	0.00	0.00	0.00	0.00	0.00	0.00	0.00	0.00	0.00	0.00	0.00
Ti	0.24	0.23	0.21	0.18	0.23	0.20	0.20	0.25	0.22	0.19	0.25	0.18	0.17	0.18
Fe^{3+}	1.17	1.16	1.11	0.98	0.90	0.85	0.81	0.82	0.91	0.96	0.85	1.04	0.51	0.62
Fe^{2+}	2.90	2.10	2.21	2.23	2.23	2.31	2.27	2.34	2.26	2.20	2.32	2.26	4.16	4.07
Mn	0.11	0.10	0.10	0.05	0.07	0.07	0.06	0.07	0.07	0.08	0.06	0.07	0.20	0.23
Mg	1.58	1.61	1.53	1.67	1.67	1.61	1.68	1.57	1.60	1.70	1.59	1.58	0.08	0.08
CaB	1.60	1.58	1.63	1.58	1.64	1.64	1.59	1.61	1.57	1.60	1.60	1.55	0.75	0.80
NaB	0.40	0.42	0.37	0.42	0.36	0.36	0.41	0.39	0.43	0.40	0.40	0.45	1.25	1.20
KA	0.19	0.18	0.18	0.14	0.16	0.17	0.16	0.17	0.15	0.14	0.17	0.14	0.28	0.25
NaA	0.24	0.25	0.21	0.18	0.27	0.27	0.25	0.26	0.24	0.21	0.30	0.21	0.58	0.59
Total cation	15.43	15.44	15.39	15.32	15.44	15.44	15.42	15.43	15.40	15.35	15.47	15.35	15.86	15.84
X_{Mg}	0.43	0.43	0.41	0.43	0.43	0.41	0.43	0.40	0.42	0.43	0.41	0.41	0.02	0.02
Si+Na+K	6.93	6.99	6.98	7.18	7.11	7.16	7.21	7.13	7.14	7.16	7.14	7.18	8.51	8.40
$Ca+Al^{IV}$	2.91	2.82	2.89	2.61	2.85	2.86	2.75	2.85	2.77	2.70	2.86	2.60	0.99	1.07

The clinopyroxene-amphibole gabbro occurs as boulders at the NE external flank at the height 1700 m. It has coarse grained texture with a cumulative tendency (Figure 2g). The paragenesis consists mainly of plagioclase, commonly weathered clinopyroxene and brown hornblende. Plagioclase (65.2 vol. %) forms labradorite large phenocrysts ($Or_{0-1}Ab_{29-33}An_{65-70}$) interlocking with each other or enclosing the hornblende crystals. The widest crystals reach 1.1 x 1.2 mm. They are frequently zoned and display mechanic twinning and kink

bands. Green hornblende (26.8 vol. %) appears as both euhedral phenocrysts (1.1 x 0.8 mm) and as interstitial anhedral crystals, which often alter into chlorite or epidote. Some of the crystals form inclusions in plagioclase. Clinopyroxene (6.8 vol. %) subhedral phenocrysts yielding the bluish or brownish colour are usually replaced by either serpentine or rarely uralite. They are augite in composition ($En_{36-48}Wo_{25-30}Fs_{22-40}$) (Table 2) according to the classification of [23].

4. Whole Rock Geochemistry

The analytical data were yielded at the CRPG, Nancy, France, using ICP-OES (Inductively Coupled Plasma-Optical Emission Spectrometry) for major elements and ICP-MS (quadrupole Mass Spectrometry) for trace elements. For whole rock analyses, samples have been first pulverized in a steel crusher and then milled to a very thin powder in an agate mill. About 300 mg of powder was fused with $LiBO_2$ and dissolved in HNO_3.

4.1. Nomenclature and Classification

The bulk rock composition (major and trace elements) and the CIPW normative composition of NBAC samples given in Table 6 reveal: (1) the occurrence of normative quartz (9.0-46.6 wt. %) in almost all felsic samples; (2) the occurrence of normative corundum (2.9-8.6 wt. %) both in all felsic volcanic rocks and in all granites (0.9-2.2 wt. %) and the lack of normative acmite in all the samples except one (I37); (3) mafic volcanic and plutonic rocks are marked by the occurrence of normative nepheline (4.1-15.5 wt. %) and normative olivine (10.6-21.8 wt. %); (4) the normative hypersthene in almost all felsic plutonic rocks samples ≤ 4.5 wt.%.

In the modified total Alkali vs. Silica (TAS) classification diagram of Le Maitre ([25]; Figure 4) plutonic unit from Ngaou Boh is made up of clinopyroxene-amphibole gabbro, alkali feldspars syenite and alkali feldspars granite whereas the volcanic suite is composed of basanite, trachyandesite, trachyte and rhyolite. The two groups are characterized by a "Daly gap" between mafic and felsic rocks, illustrating a lack of intermediate terms. All the analyzed NBAC rocks plot over the alkaline-subalkaline boundary [26] except two samples: gabbro TG24 and rhyolite I35.

The agpaitic index [A.I = $(Na_2O + K_2O)/Al_2O_3$ mole %] is mainly < 1 (0.19-0.97) except for two samples (granite I34 and syenite I37= 1) which can be considered as peralkaline. Basanites, clinopyroxene-amphibole gabbros and granitic rocks are metaluminous (0.50≤ ASI ≤ 0.99) while all felsic volcanic rocks are peraluminous (ASI ≥ 1.03-1.32) ([27,28]; Figure 5). The ASI is Alumina Saturation Index: molar % $Al_2O_3/CaO + Na_2O + K_2O$.

The NBAC gabbros and granitoids plot in the field of I-type granite ([29]; Figure 5). However, granitoids display characters of A-type granite and they plot in the domain of ferroan rocks whereas gabbros are assigned to magnesian rocks ([30]; Figure 6a). Moreover, in the MALI vs. silica diagram ([30]; Figure 6b) clinopyroxene-amphibole gabbros exhibit calcic affinity; syenites are strictly alkalic while granites display mainly alkali-calcic and alkalic features.

Table 6. Major elements (wt. %), trace elements, rare earth elements (ppm) and CIPW norm (wt. %) data for representative samples of the NBAC. The samples concerned by this investigation are quite fresh; those with LOI (loss on ignition) > 3% have been excluded. Fe_2O_t = Fe_2O_3 total. For CIPW norms calculation, the values of Fe_2O_3/FeO ratios are indicated

Rock type	Basanite			Trachyandesite	Trachyte		Rhyolite	Gabbro		Syenite		Granite		
Sample	I31	HG5	HG16	I42	TG21	TG20	I33	TG23	TG24	I38	I37	I32	I30	I34
SiO_2	42.65	42.73	42.21	61.66	69.55	70.14	75.46	48.77	50.15	60.99	61.23	66.38	66.91	68.23
TiO_2	3.66	3.00	2.74	1.44	0.12	0.15	0.20	0.30	0.29	0.44	0.95	0.72	0.58	0.24
Al_2O_3	14.02	13.00	12.24	14.68	16.07	15.32	10.65	22.98	25.86	18.81	15.25	14.88	14.71	14.67
Fe_2O_3t	12.41	12.58	12.82	6.31	2.87	2.70	4.78	5.52	3.57	2.74	4.48	4.84	5.00	3.84
MnO	0.18	0.21	0.21	0.08	0.00	0.04	0.00	0.05	0.04	0.73	0.15	0.12	0.08	0.13
MgO	9.44	10.8	11.66	2.73	0.00	0.25	0.00	5.25	2.92	0.64	2.86	0.90	0.73	0.05
CaO	11.31	9.73	11.72	4.13	0.40	0.50	0.00	11.47	13.24	1.60	2.39	2.05	1.84	0.40
Na_2O	3.24	3.42	3.59	3.35	3.66	4.78	3.49	4.10	2.75	5.83	5.01	4.47	4.39	5.55
K_2O	1.73	1.72	1.15	3.90	4.98	4.92	4.25	0.98	0.36	6.06	6.50	4.19	4.65	5.01
P_2O_5	0.68	1.01	0.85	0.46	0.03	0.03	0.00	0.02	0.06	0.18	0.27	0.26	0.21	0.04
LOI	0.67	0.87	0.15	0.87	2.00	0.95	1.10	1.52	1.02	1.98	0.32	1.03	0.78	0.63
Total	99.99	99.06	99.34	99.62	99.68	99.77	99.93	100.96	100.26	100.04	99.41	99.83	99.88	98.75
Fe_2O_3/FeO	0.15	0.15	0.15	0.40	0.40	0.40	0.40	0.35	0.35	0.35	0.40	0.40	0.40	0.40
CIPW norm wt %														
Quartz	0	0	0	16.6	42.4	27.17	46.62	0	2.20	9.03	0	20.86	19.90	18.50
Plagioclase	24.41	26.25	15.44	40.33	10.51	33.43	16.42	68.44	80.35	38.48	40.47	39.78	39.97	42.70
Orthoclase	10.66	10.60	7.30	23.85	29.58	29.15	25.12	5.94	2.27	35.96	40.30	25.20	27.84	29.68
Corundum	0	0	0	0.41	8.61	3.48	2.86	0	0	4.74	0	2.19	1.35	0.93
Nepheline	11.59	9.49	15.48	8.75	0	0	0	4.11	0	0	0	0	0	0
Diopside	23.43	17.21	30.64	0	0	0	0	4.66	1.41	0	6.45	0.00	0	0
Hypersthene	0	0	0	0	1.76	2.24	2.83	0	9.00	4.37	4.22	4.47	4.31	2.50
Olivine	16.18	21.77	19.18	0	0	0	0	10.60	0	0	1.42	0	0	0
Acmite	0	0	0	0	0	0	0	0	0	0	1.69	0		0
Ilmenite	6.95	5.70	5.20	2.73	0.23	0.28	0.38	0.57	0.55	0.84	1.80	1.37	1.10	0.46

Rock type	Basanite			Trachyandesite	Trachyte		Rhyolite	Gabbro		Syenite		Granite		
Sample	I31	HG5	HG16	I42	TG21	TG20	I33	TG23	TG24	I38	I37	I32	I30	I34
Magnetite	2.70	2.74	2.78	3.65	1.67	1.57	2.77	2.80	1.81	1.39	1.75	2.81	2.90	2.23
Hematite	0	0	0	0	0	0	0	0	0		0	0	0	0
Apatite	1.58	2.34	1.97	1.07	0.07	0.07	0	0.05	0.14	0.42	0.63	0.6	0.49	0.09
Trace (ppm)														
Cr	425.00	393.10	688.10	85.06	0	0	0	129.95	49.10	0	0.02	6.05	0	0
Co	45.90	48.61	52.98	16.73	0.47	0.33	0.47	39.12	17.40	0.41	12.00	5.93	4.36	0.27
Ni	144.00	336.3	252.00	39.47	0	0	0	54.52	18.95	0	48.00	0	0	0
V	270.00	193.4	244.10	106.50	0	0	0	74.00	57.39	7.76	96.00	26.73	13.20	0
Cu	44.30	68.03	71.10	21.22	0	4.01	0	5.75	21.65	0	0	0	0	0
Zn	109.00	124.5	119.80	114.90	91.80	86.79	237.00	55.38	30.85	147.60	214.80	130.40	121.00	214.80
Ga	20.40	21.43	18.68	26.15	38.10	39.04	43.4	18.45	19.90	29.27	23.70	28.32	31.00	43.20
Ge	1.40	1.30	1.51	1.578	1.62	2.27	2.48	1.00	1.53	1.78	2.00	1.61	1.78	2.19
As	0	1.30	0	0	0	0	0.84	0	0	7.65	0	0	0	0
Be	1.68	2.37	1.60	2.78	5.26	7.43	12.8	0	0	5.57	21.00	9.24	5.98	6.53
Cs	0.38	0.378	0.64	2.41	0.81	0.72	0.65	0.56	0	1.43	7.70	1.14	0.85	0.49
Rb	38.80	44.66	94.77	190.10	134.90	128.60	195.00	14.35	5.66	161.60	291.90	160.90	142.00	105.00
Sr	843.00	1069.00	951.10	545.30	72.77	63.40	6.80	769.89	710.10	101.50	981.90	197.00	165.00	13.69
Ba	546.10	533.8	626.70	1016.00	139.4	132.10	20.60	159.57	172.90	186.60	2324.00	550.90	411.00	110.8
Zr	277.00	348.8	253.80	401.40	550.00	525.20	2866.00	13.45	28.70	1029.00	650.90	514.60	539.00	1065.00
Hf	6.14	7.40	5.58	9.25	17.53	15.95	66.30	0.32	0.73	21.00	12.90	12.83	14.8	24.36
Ta	5.02	5.62	6.26	0.87	13.71	13.09	20.20	0.28	0.27	16.31	4.70	7.86	7.35	13.65
Nb	67.10	81.68	91.86	13.30	175.90	172.70	262.00	1.30	2.58	226.6	47.2	60.98	90.7	180.20
Y	29.20	34.66	26.76	15.35	39.33	61.03	92.40	3.34	3.99	41.72	20.28	72.81	52.8	76.93
Mo	2.34	3.63	3.27	1.42	4.26	1.37	0.71	0	0	21.51	6.67	2.89	4.79	22.67
Cd	0	0.37	0.34	0.28	0	0.00	0.82	0	0	1.02	0.50	0.49	0.52	0.83
In	0.10	0.11	0.11	0.00	0.17	0.15	0.24	0	0	0.00	0.19	0.12	0.12	0.24
Sn	2.00	2.51	1.65	3.55	9.38	8.79	17.50	0	0	2.91	4.00	4.79	7.03	7.33
Sb	0	0.11	0.12	0.24	0	0	0.24	0.35	0	0.61	0	0	0	0
La	45.60	59.2	68.56	97.29	100.1	321.20	27.3	3.20	5.86	159.80	86.8	55.58	89.60	88.99
Ce	92.80	120.80	128.70	188.30	147.20	262.80	53.00	6.35	9.05	258.80	198.50	113.50	180.00	262.30
Pr	11.80	14.61	14.50	19.60	27.40	77.47	6.50	0.81	1.20	24.59	14.12	13.94	20.80	24.74
Nd	48.60	59.07	54.85	66.12	92.38	262.10	23.60	3.43	5.53	73.70	50.19	54.20	76.10	89.69
Sm	9.92	11.70	9.90	9.39	17.55	47.43	6.14	0.81	1.16	10.24	12.60	11.87	15.10	18.89
Eu	3.28	3.71	3.30	2.05	1.35	3.38	0.36	0.72	0.79	2.31	1.63	2.29	2.35	1.66
Gd	8.75	9.83	8.04	5.94	10.77	28.60	9.60	0.76	0.96	7.66	10.51	11.45	11.90	14.94
Tb	1.13	1.37	1.08	0.73	1.9	4.26	2.34	0.10	0.16	1.18	0.91	1.91	1.90	2.54
Dy	5.89	7.105	5.63	3.36	10.27	20.44	18.90	0.69	0.84	6.81	11.12	11.51	10.70	15.15
Ho	1.07	1.22	0.95	0.52	1.69	2.92	4.41	0.11	0.19	1.30	2.50	2.24	1.92	2.88
Er	2.73	3.14	2.38	1.36	4.52	7.13	12.20	0.29	0.38	3.97	8.98	6.41	5.14	8.28
Tm	0.37	0.43	0.31	0.18	0.67	0.96	1.99	0.06	0.11	0.60	0.29	0.96	0.74	1.23
Yb	2.23	2.67	1.92	1.11	4.46	6.04	12.70	0.31	0.38	4.21	5.70	6.48	4.85	8.31
Lu	0.33	0.39	0.29	0.16	0.62	0.80	1.72	0.03	0.06	0.66	0.85	0.93	0.73	1.21
Bi	0	0	0	0.11	0	0	0.21	0.01	0	0	0	0	0	0
W	0.41	0.78	1.05	0.83	2.63	2.21	0.51	0.28	0.00	5.19	5.70	2.30	1.97	0.83
Pb	2.47	3.64	3.68	11.48	6.78	6.04	27.50	5.01	2.25	12.70	7.58	7.90	8.96	8.10
Th	4.35	6.27	7.97	35.74	25.33	23.78	35.20	0.35	0.57	23.55	55.20	15.72	17.70	16.72
U	1.22	1.80	1.98	2.85	5.84	4.57	9.72	1.05	0.10	5.99	4.85	4.94	3.84	5.77
∑REE	234.49	295.25	300.42	396.10	420.88	1045.53	180.76	17.67	26.67	555.84	404.70	293.26	421.83	540.81
Eu/Eu*	1.05	0.52	0.56	0.78	0.28	0.26	0.14	2.75	2.22	0.76	0.42	0.59	0.52	0.29
$(La/Yb)_N$	13.89	2.31	3.72	59.33	15.25	36.13	1.46	7.01	10.48	25.77	10.34	5.83	12.55	7.27
$(Dy/Lu)_N$	1.81	81.25	87.21	2.10	1.66	2.56	1.10	2.30	1.40	1.46	1.24	1.25	1.31	1.03
Mg#	60.11	62.97	64.32	46.11	0	15.36	0.00	65.33	61.80	31.50	55.88	26.94	22.50	2.47
A/CNK	0.50	0.52	0.43	0.85	1.32	1.09	1.03	0.80	0.89	0.99	0.78	0.95	0.94	0.96
A/NK	1.95	1.74	1.71	1.50	1.41	1.16	1.03	2.94	5.26	1.17	1.00	1.25	1.20	1.00
A.I	0.51	0.57	0.58	0.67	0.71	0.86	0.97	0.34	0.19	0.85	1.00	0.80	0.83	1.00
Tsat zircon	607	629	555	822	929	900		541	601	873	878	957	846	937
Tsat apatite	757	842	788	1006	806	804		493	606	981	959	813	925	882

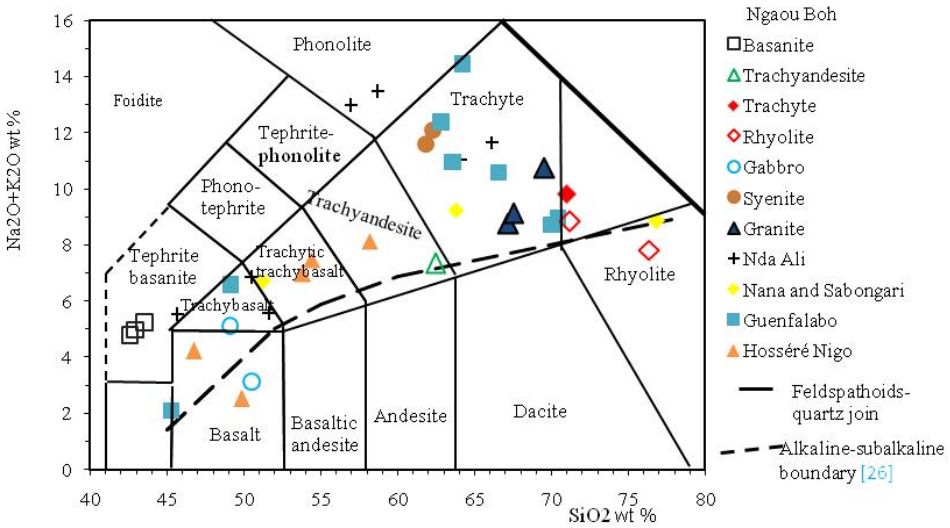

Figure 4. Total Alkali vs. Silica diagram ([25] modified) for the NBAC rocks and some anorogenic complexes from the CL for comparison: Nda Ali [9], Hosséré Nigo [14], Hosséré Guenfalabo [15], Nana and Sabongari [10,11]

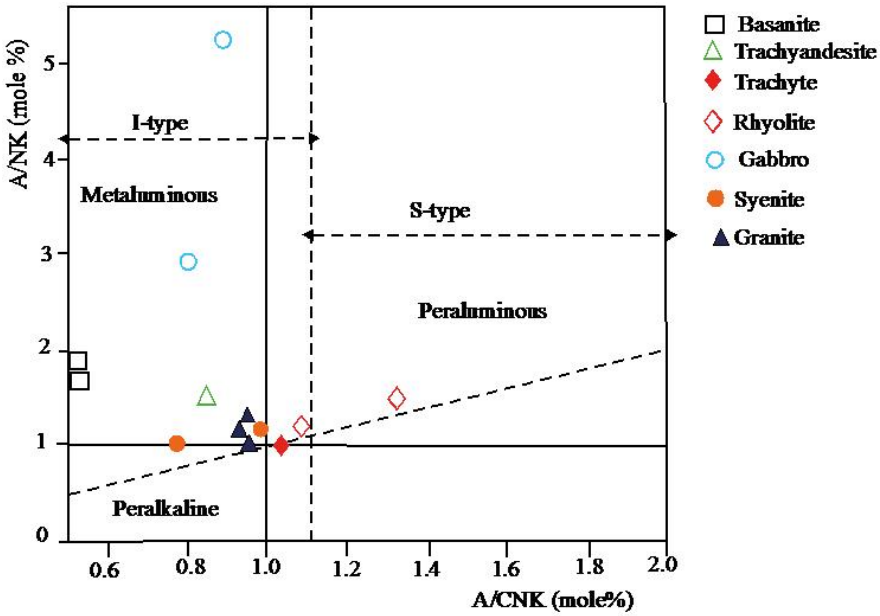

Figure 5. NBAC rocks in the molar % A/NK (Al_2O_3/Na_2O+K_2O) vs. molar % A/CNK ($Al_2O_3/CaO+Na_2O+K_2O$) diagram of [27]. Peraluminous and metaluminous fields after [27]; fields of I-type and S-type granitoids after [29]. Mafic rocks are also plotted for comparison

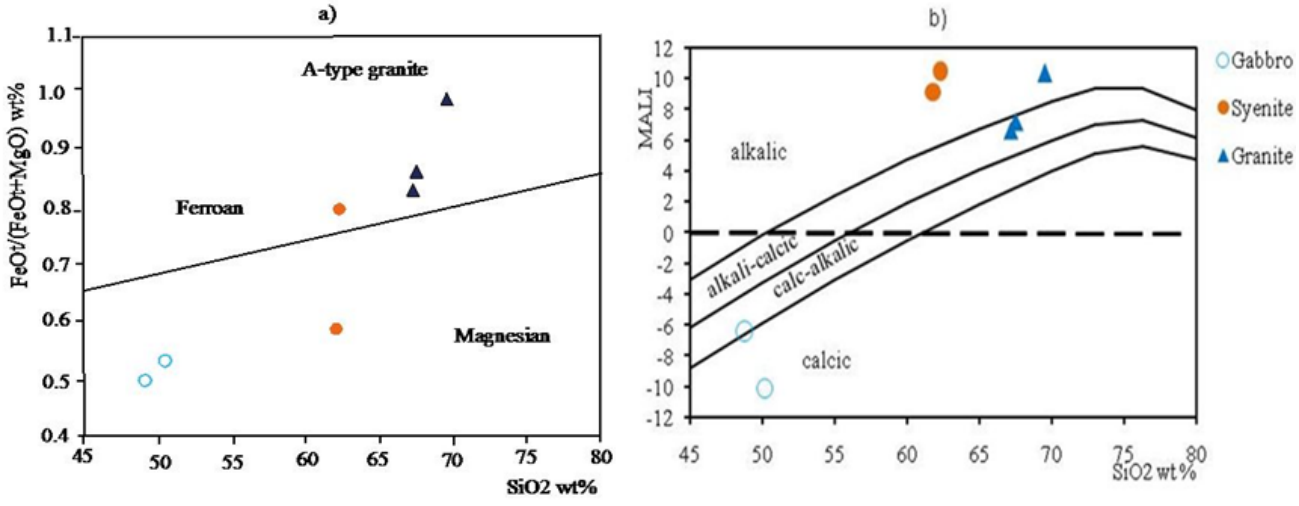

Figure 6. Plutonic rocks from NBAC subdivided into: (a) ferroan (A-type granite) and magnesian types; (b) alkalic, alkali-calcic, calc-alcalic and calcic in the MALI (CaO wt. %- (NaO_2 wt. %+K_2O wt. %)) against silica diagram [30]

4.2. Major Elements Characteristics

Basanites display low SiO_2 (42.2-42.7wt. %) and high Al_2O_3 (12.2-14.0 wt. %), Fe_2O_3t (12.4-12.8 wt. %) and CaO (9.7-11.7wt. %). The K_2O/Na_2O ratio (~ 0.5) indicates their sodic character, which is different with the majority of the studied plutonic-volcanic massifs of the CL, rather potassic [3,4]. Biotite-clinopyroxene trachytes and clinopyroxene-amphibole rhyolites have high SiO_2 (69.6-75.5 wt. %), Al_2O_3 (10.7-16.1wt. %), low Fe_2O_3t (2.7-4.8 wt. %), CaO (0.0-0.5 wt. %), moderate Na_2O (3.5-4.8wt. %) and K_2O (4.3-5.0 wt. %). K_2O/Na_2O ratios range from 1.03-1.36 reflects its potassic character. Gabbros have low to moderate SiO_2 (48.8-50.2 %), Fe_2O_3t (3.6-5.5 wt. %), MgO (2.9-5.3 wt. %), high Al_2O_3 (23.0-25.9 wt. %) and CaO (11.5-13.2 wt. %) contents. In the other hand, high but narrow variation in SiO_2 (61.0-68.2 wt. %), Al_2O_3 (14.7-18.8 wt. %), Fe_2O_3t (2.7-5.0wt. %) and low CaO (0.4-2.4 wt. %) characterize the NBAC felsic plutonic rocks. The K_2O/Na_2O ratios range from 0.9 to 1.3. The molar Mg number [$Mg^{\#}$= (molar 100 x $Mg/(Mg+Fe^{2+})$] up to 66 for all the samples decreases with the increasing of SiO_2.

The major elements variations diagrams (Figure 7) display: i) linear positive trends for Na_2O, K_2O, negative for CaO, MgO and Al_2O_3; and ii) a lack of correlation for the other oxides Fe_2O_3, TiO_2, P_2O_5 with the increasing of SiO_2.

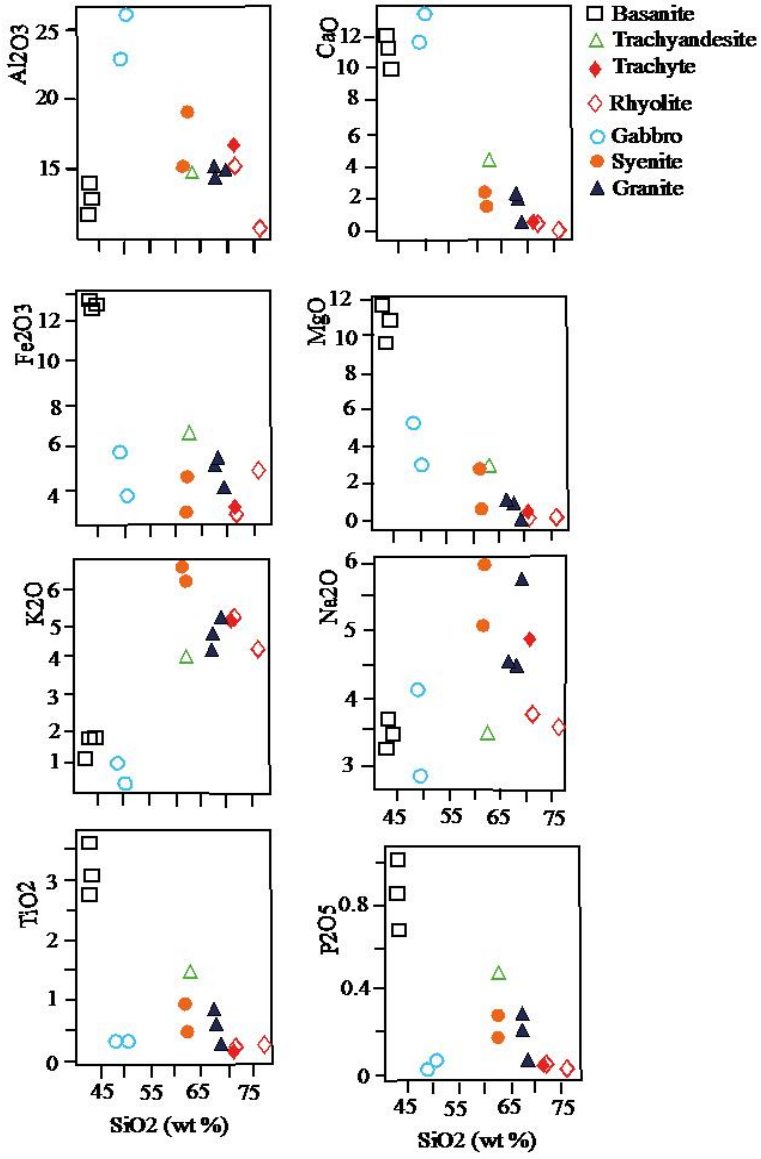

Figure 7. Harker variation diagrams for some major elements

4.3. Trace Elements Characteristics

Compatible elements of clinopyroxene-amphibole gabbros and mafic lavas such as Ni (19.0-336.3 ppm), Co (17.4-53.0 ppm), Cr (49.1-688.1 ppm) and V (57.4-270.0 ppm) have relative high contents. Conversely, granitoids and felsic lavas contents of incompatible elements are higher than those of compatible elements: Ba (159.6-2324.0 ppm), Zr (514.6-2866.0 ppm), Rb (134.9-291.9 ppm), Sr (6.8-981.9 ppm) and Y (20.3-92.4 ppm) (Table 6).

Trace elements of all NBAC rocks as Ta, Nb, Rb display clear chemical trends with Th, and there is a lack of correlation between Sr, Zr, and La with Th (Figure 8). Compatible transition elements (Ni and Cr) decrease with the increasing of Th might reflect the fractionation of olivine and clinopyroxene.

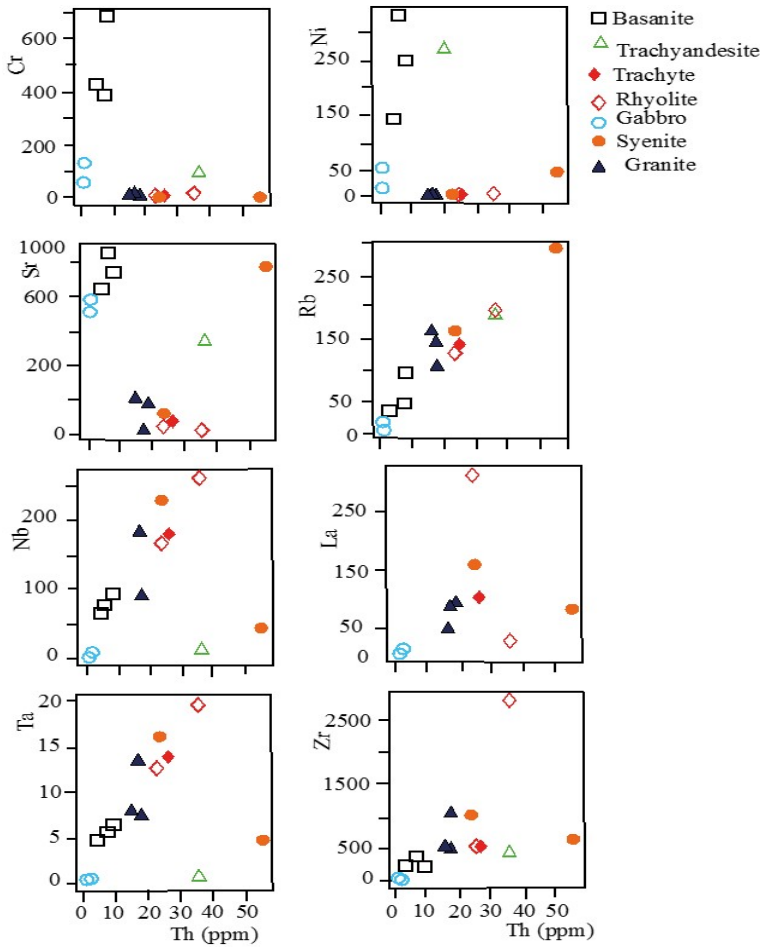

Figure 8. Harker variation diagrams for some trace elements

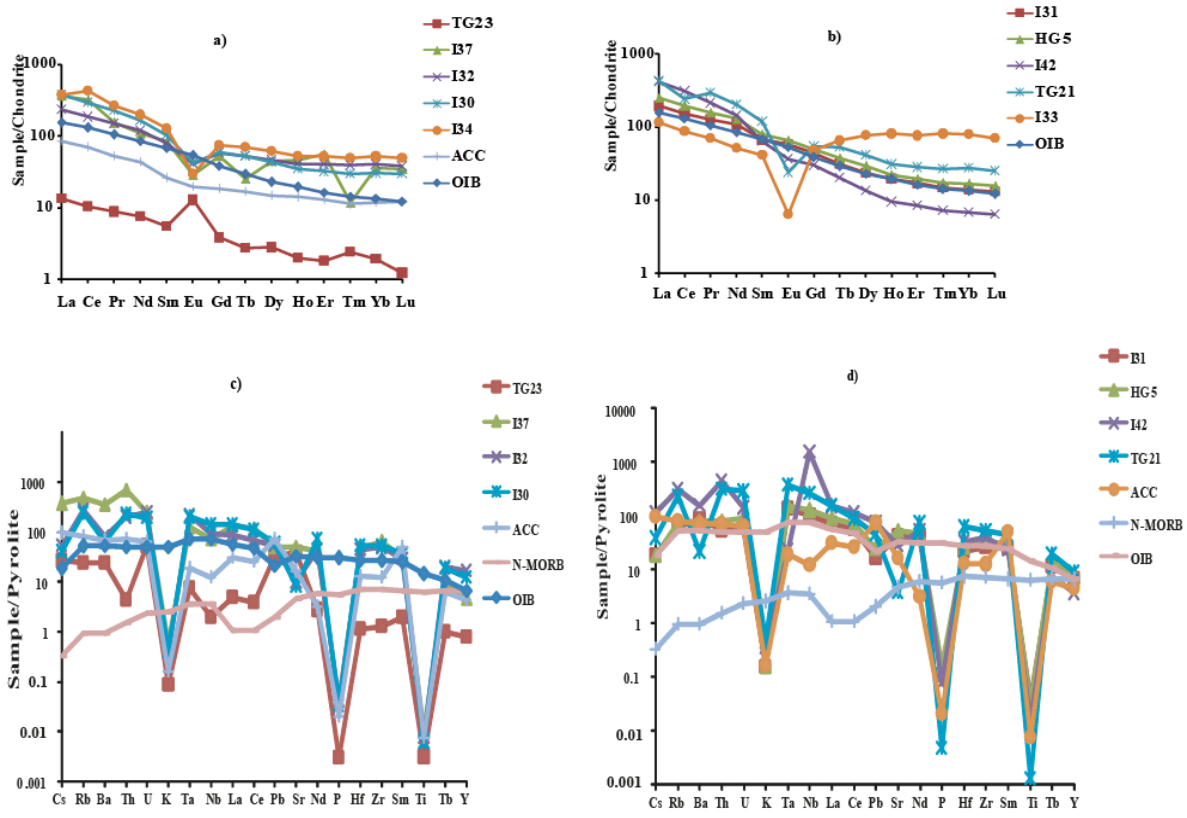

Figure 9. Chondrite normalized REE patterns of plutonic rocks (a) and volcanics (b) from NBAC (Chondrite values after [31]. ACC=Average Continental Crust after [32]); OIB composition from [33]. Pyrolite normalized spidergrams of plutonic rocks (c) and volcanics (d) from NBAC (Pyrolite values after [31]. ACC=Average Continental Crust [32]; OIB and N-MORB compositions from [33]

Chondrite-normalized patterns of NBAC alkali feldspars granites and alkali feldspars syenites show a pronounced enrichment in light rare earth elements (LREE) relative to heavy rare earth elements (HREE) while clinopyroxene-amphibole gabbros are characterized by a moderate enrichment in LREE relative to HREE (Figure 9a). The overall $(La/Yb)_N$ ratio (5.83-25.77) highlights the moderate to strong fractionation of LREE/HREE whereas $(Dy_N/Lu)_N$ ratio (1.03-1.46) suggests the lower MREE/HREE fractionation. The I34 sample has the highest LREE enrichment (~500 times) relative to chondrite (Figure 9a). The ∑REE of granites vary very few (293.26-540.81ppm). All their REE patterns have slight negative Eu anomalies (Figure 9a) evidenced by Eu/Eu* < 1 (0.30-0.60). The REE patterns of the Ngaou Boh gabbros (∑REE=17.67-26.67 ppm) are very different from those of granites; they have moderate LREE/HREE with $(La/Yb)_N$ ratios ranging from 7.01 to 10.48 and show extreme positive Eu anomalies (Eu/Eu* = 2.22-2.75) indicative of cumulus plagioclase. The pyrolite normalized incompatible trace elements profiles (Figure 9c) of plutonic rocks exhibit slight spikes in Rb, Th, Zr and strong negative anomalies at K, P, Ti.

The chondrite normalized patterns of biotite-clinopyroxene trachytes and clinopyroxene-amphibole rhyolites display prominent negative Eu anomalies (Eu/Eu*=0.14-0.28) indicative of the significant fractionation of feldspars (Figure 9b). The $(La/Yb)_N$ (1.46-36.13) and $(Dy/Lu)_N$ (1.10-2.56) ratios respectively testify the low enrichment of LREE/HREE and MREE/HREE. Chondrite-normalized REE patterns of basanites (Figure 9b) display slight LREE enrichment relative to HREE ($(La/Yb)_N$= 2.31-13.89) illustrated by an almost flat profile for heavy rare earth elements. In other words, the shape of the patterns of basanite describes a profile of moderate slope from LREE to HREE, which reflects an enrichment of 90 to 200 times compared to the chondrite. Rhyolites and trachytes are characterized by high REEs contents, with ∑REE ranging between 180.96 and 1045.53 ppm.

The pyrolite-normalized spidergrams of NBAC trachytes display strong negative K, P and Ti anomalies and moderate negative Ba and Sr (Figure 9; c and d). K, Ba and Sr anomalies reflect significant fractionation of alkali feldspars, while Ti anomaly is symptomatic of Fe-Ti oxides fractionation.

5. Discussion and Concluding Remarks

5.1. Geodynamic Setting

The NBAC rocks have an affinity with Within-Plate Granites (WPG) except clinopyroxene-amphibole gabbros and biotite-clinopyroxene trachytes in the Rb vs. Y+Nb geotectonic diagram [34] (Figure 10a). According to the Ce-Y-Nb discriminating diagram of [35] all the studied granitoids are of A-type granite [36] and plot both in the A1 and A2-subtype fields (Figure 10b): A-type granite is known as related to a post-collision environment or a typical anorogenic environment with the possible presence of "rapakivi-type granite". Moreover, a synthetic review of the position of NBAC rocks in the $(Nb/Zr)_N$ vs. Zr discriminating diagram ([37]; Figure 10c), and the Th/Hf vs. Ta/Hf, Th/Ta vs. Yb and Th/Ta vs. Ta/Yb variation diagrams of [38,39]; Figure 10d-f) leads to the conclusion that an alkaline and typically anorogenic or post-collisional magmatism characterizes the NBAC and results in a relic signature of the subduction type. The studied NBAC samples plot in four different fields: within plate zone (WPG), the post-collision zone (PCG), the within plate volcanic zone (WPVZ) and the active continental margin (ACM) field.

5.2. Magma Sources

It is recognized that mafic magmas have two main sources: the subcontinental lithosphere mantle (SCLM) and the upper mantle. [42] characterized these two sources by the La/Ta> 22 and La/Nb> 1.5 ratios for magmas from the SCLM; La/Ta < 22 and La/Nb< 1.5 ratios for those originated from the upper mantle. Therefore, the La/Ta (8.8-10.9) and La/Nb (0.68-0.75) ratios indicate an asthenospheric source for basanites parent magmas. The same ratios La/Ta (10.4-21.7) and La/Nb (2.3-2.5), on the other hand, evidence a hybrid source (both the upper mantle and the SCLM) for gabbros parent magmas.

Basanites are characterized by moderate MgO (9.44-11.66 wt. %) and compatible elements contents (Ni: 144.00-336.30 ppm, Cr: 393.10-688.10 ppm). Such values are relatively sufficient to be regarded as indicators of primary liquids directly resulting from the mantle melting according to [43]. These basanites nevertheless represent primary melt that has early undergone differentiation process. The overall studied samples have OIBs features (Figure 9); this is testified by their average La/Nb (0.71) and Nb/Ta (14.2) ratios similar to the respective OIB values which are 0.77 and 17.7 [34].

At least two distinct magmatic sources have controlled the formation of the NBAC rocks and the two subsequent series (Figure 11). The clinopyroxene-amphibole gabbro-alkaline syenite (trachyte)-alkaline granite- suite originates from the partial melting of upper mantle spinel peridotite (with slightly higher $(La/Yb)_N$ ratios:7.0-36.1; average~21.6). Indeed, mantle origin is ascribed in general to metaluminous, alkaline or peralkaline granitoids. Such rocks match with peralkaline and alkaline granitoids (PAG) or within plate granite (WPG) and A-type granitoids [31,45]. The NBAC plutonic rocks are mainly metaluminous (A/CNK<1) with geochemical features of I-type granites. Such igneous rocks have been described as related to partial melting of a magmatic protolith [46,47]. [36] established that A-type granites derived from transitional or alkaline mafic mantle sources while [48] argued mantle-derived intrusions inferred partial melt of the lower crust for the petrogenesis of A-type granites.

On the other hand, the basanite-trachyandesite-rhyolite suite originates from the upper mantle garnet peridotite (Figure 11) (with lower $(La/Yb)_N$ ratios: 1.46-13.83; average~7.6). The relative narrow Nb/Ta (4.64-9.55; average~ 7.1) and high La/Nb (0.57-1.86; average~ 1.22) ratios of clinopyroxene-amphibole gabbros also confirm that they derive from a mantle source distinctly different from that of basanitic rocks, although that source compositionally close to OIB component according the pyrolite-normalized spidergrams (Figure 10). Moreover,

clinopyroxene-amphibole gabbros tend to be more primitive in regard with lower content in alkalis (NaO_2, K_2O) and higher contents in CaO than basanites (Table 6). Overall, the mantle origin is commonly reported for almost all the studied anorogenic complexes of the CL ([4,10] and references therein).

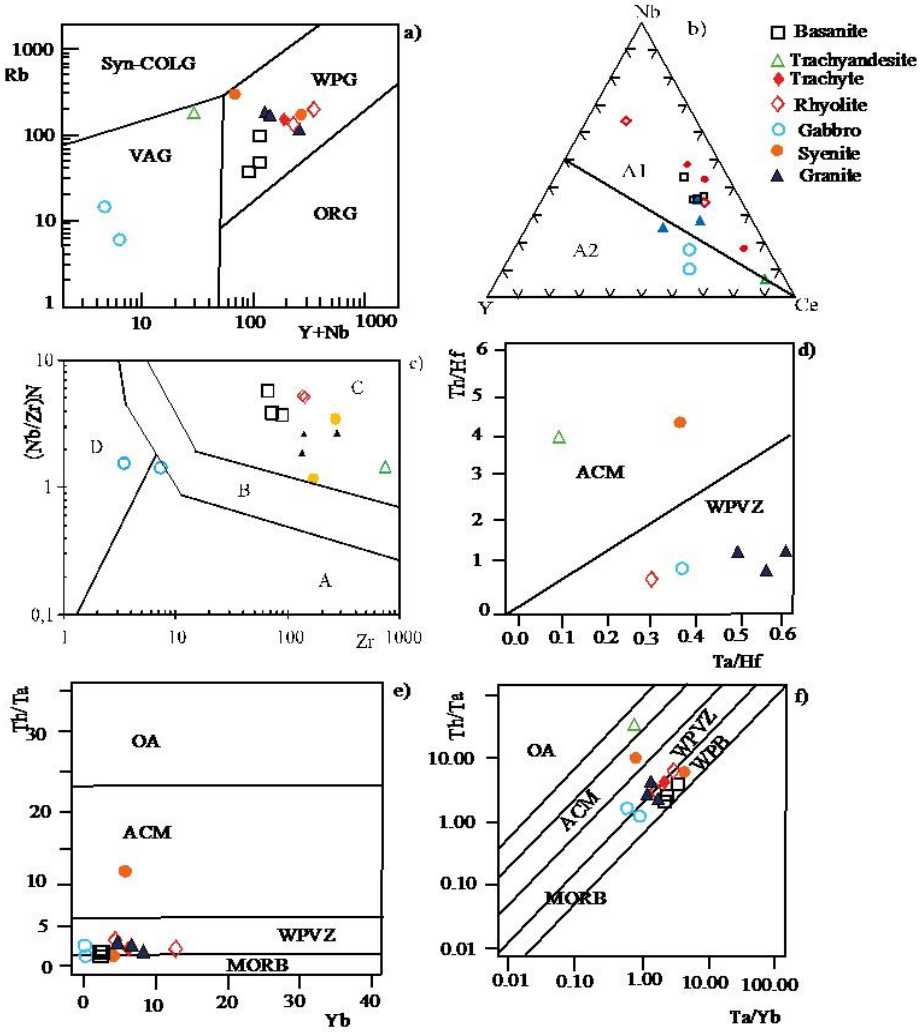

Figure 10. Geotectonic setting for felsic rocks and mafic rocks also plotted for comparison. (a) Rb vs. Y+Nb diagram [34] (b) Ce-Y-Nb discriminating diagram after [35]: A1= field of Oceanic Island basalts, A2= field of Post orogenic rocks or Island Arc basalts; (c) $(Nb/Zr)_N$ vs. Zr diagram [37]. Normalizing values from [31]. A= magmatic rocks related to subduction zone (VAG); B= Granitoids associated to collision zone (PCG); C= Alkaline rocks from intraplate zone (WPG); D= Syn-collisional granites. (d) Th/Hf vs. Ta/Hf diagram: different domains after [40,41], OA= Oceanic arcs, ACM= Active continental margins, WPVZ= Within plate volcanic zone, WPB= Within plate basalts, MORB= Mid-ocean ridge basalts; (e) Th/Ta vs. Yb diagram: discriminating lines after [38]; (f) Th/Ta vs. Ta/Yb diagram: line separating the two domains after [39]

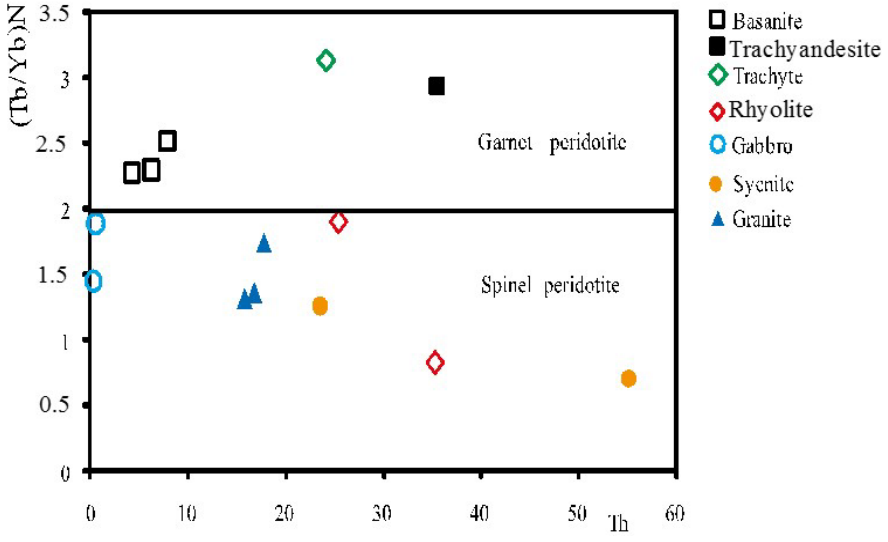

Figure 11. $(Tb/Yb)_N$ vs. Th diagram distinguishing the melting of garnet peridotite from that of spinel peridotite [44]. Normalizing values from [32]

5.3. Magma Differentiation Processes

5.3.1. Fractional Crystallization/Crustal Contamination?

The major and most trace elements behavior allows to decipher the petrogenesis and magma processes of the NBAC. The linear positive or negative correlations of major elements in the Harker variation diagrams such as Na_2O, K_2O, Fe_2O_3t, CaO and MgO vs. SiO_2 wt % (Figure 7) corroborates the fractionation of main mineral phases during the differentiation process, and evidence two magmatic series. Thereby, trachyandesites, biotite-clinopyroxene trachyte and clinopyroxene-amphibole rhyolites might likely related to basanites by the fractionation of alkali feldspars with regard to their pronounced negative Eu anomalies (Eu/Eu*= 0.14-0.80) whereas alkali feldspar syenites and alkali feldspar granites derived from mafic parental liquid, with clinopyroxene-amphibole gabbro as primitive liquids, by the fractionation of alkali feldspars, plagioclases, ca-pyroxenes and amphiboles.

The LILE vs. HFSE (Rb, Pb, U, vs. Th) and HFSE vs. HFSE (Nb, Zr vs. Th) diagrams underline a positive linear correlation passing through the origin (Figure 8). Such correlations are consistent with magma evolving by fractional crystallization mechanism [49]. Whatever are those prior analyses, the awaited Sr-Nd-Pb isotopic compositions, undoubtedly must unravel these features.

The almost perfect parallelism between the chondrite-REE normalized patterns of alkali feldspar syenites and those of alkali feldspar granites (Figure 9a and Figure 9b) correlated to the constant variation of the trace elements ratios, for instance $(La/Yb)_N$ (5.8-25.8), is also the result of a magmatic differentiation marked by fractional crystallization [50]. The magmatic affinity and the diversity of the NBAC rocks, though, evidences several mantle components and the involvement of differentiation processes. Therefore, the parallelism of REE chondrite-normalized patterns of mafic and felsic lavas testifies their co-genetic link despite the apparent "Daly gap", except the rhyolite I35 which could be either the result of partial melt of a crustal component or of crustal contamination of mafic magma during its ascension [16].

However, the lack of significant depletion in Nb, Ta, P and Ti combined to the faintly enrichment in Ba and Th suggest that mantle-derived parent magmas were not strongly modified by crustal materials (Figure 9c and Figure 9d). No constraint of magma mixing characteristics has been found (zoned crystals or enclaves). Consequently, fractional crystallization is the main differentiation process responsible of the NBAC magmatic evolution in spite the apparent "Daly gap" [17,51].

5.3.2. Thermobarometry

The determination of P and T crystallization conditions was achieved using zircon and apatite saturation thermometers of [52] and [53]. The estimated temperature and pressure are presented in Table 6. We consider that zircon is not liquidus phase for basanites contrary to apatite which might crystallize from the liquidus or at temperature below. On the other hand, assuming that clinopyroxene-amphibole gabbros are more or less cumulative phases, their zircon and apatite saturation temperatures are not significant. Trachytes with higher zircon saturation temperatures (930-900°C) than those of apatite (806-804°C) begin to crystallize as liquidus, indicating that zircon saturation has been achieved. The granitoids have a wide range of zircon saturation temperatures (957-846°C) that are lower or higher than those of apatite (981-925°C), showing that they are either liquidus phases or have crystallized slightly below liquidus. The ilmenite-magnetite and ilmenite-hematite geothermobarometers [54,55] indicate the following temperatures ranges: 734-770°C for basanite and 598-925°C for alkali feldspar granite. The same geothermobarometer allows estimating oxygen fugacities ranging from -16 to -17 (basanite) and -22 to -12 (alkali feldspar granite).

Finally expected isotopic, petrological and geochronological (notably U-Pb) data will undoubtedly provide more precision in the knowledge of the detailed NBAC petrogenetic model.

Acknowledgments

This paper is dedicated to late Junior Désiré Nolla who passed in glory in July 2017 for his encouragements and friendly support during the early moments of this work. The authors are grateful to the *Ministère des Affaires Étrangères* of France for the financial support of one of the mission works on NBAC and for providing a scholarship to I.Z. for his PhD study at the *Université Paris-Sud Orsay (now Paris-Saclay).*

References

[1] Nkono, C., Féménias, O., Demaiffe, D., "Geodynamic model for the development of the Cameroon Hot Line (Equatorial Africa)", *Journal of African Earth Sciences*, 100, 626-633, 2014.

[2] Déruelle, B., Ngounouno, I., Demaiffe, D., "The ''Cameroon Hot Line" (CHL): a unique example of active alkaline intraplate structure in both oceanic and continental lithospheres", *Comptes Rendus Geosciences*, 339, 589-600, 2007.

[3] Nkouathio, D.G., Kagou Dongmo, A., Bardintzeff, J.M., Wandji, P., Bellon, H., Pouclet, A., "Evolution of volcanism in graben and horst structures along the Cenozoic Cameroon Line (Africa): implications for tectonic evolution and mantle source composition", *Mineralogy and Petrology*, 94, 3-4, 287-303, 2008.

[4] Njonfang, E., Nono, A., Kamgang, P., Ngako, V., Tchoua M.F., "Cameroon Line magmatism (central Africa): a reappraisal", *in Beccaluva, L., Bianchini, G., Wilson, M. (Eds.), Volcanism and Evolution of the African Lithosphere: Geological Society of America Special Paper, vol. 478. The Geological Society of America, Inc.*, 173-191, 2011.

[5] Lasserre, M., "Mise au point sur les granitoïdes dits "ultimes" du Cameroun: gisement, pétrographie et géochronologie", *Bull. B.R.G.M.*, 2è série, IV, n°2, 143-159, 1978.

[6] Jacquemin, H., Sheppard, S.M.F., Vidal, P., "Isotopic geochemistry (O, Sr, Pb) of the Golda Zuelva and Mboutou anorogenic complexes, North Cameroon: mantle origin with evidence of crustal contamination", *Earth and Planetary Science Letters*, 61, 97-111, 1982.

[7] Ghogomu, R.T., Moreau, C., Brown, W.L., Rocci, G., "The Ntumbaw complex, NW Cameroon: an atypical anorogenic ring complex of intermediate composition", Journal of African Earth Sciences, 8, 1-9, 1989.

[8] Kambou, R., Nzenti, J.P., Soba, D., "Apport à la connaissance des complexes anorogéniques d'âge tertiaire de la Ligne du Cameroun: le complexe pluto-volcanique de Tchégui (Nord-Cameroun)",

Comptes Rendus de l'Académie des Sciences, 308, 1257-1260, 1989.

[9] Njonfang, E., Moreau, C., "The mineralogy and geochemistry of a subvolcanic alkaline complex from the Cameroon Line: The Nda Ali massif, southwest Cameroon", *Journal of African Earth Sciences*, 22, 2, 113-132, 1996.

[10] Njonfang, E., Tchuenté Tchoneng, G., Cozzupoli, D., Lucci, F., "Petrogenesis of the Sabongari alkaline complex, Cameroon line (central Africa): Preliminary petrological and geochemical constraints", *Journal of African Earth Sciences*, 83, 25-54, 2013.

[11] Njonfang, E., Laurenzi, M.A., Wokwenmendam Nguet, P., Cozzupoli, D., "^{40}Ar-^{39}Ar ages from the Sabongari and Nana igneous complexes within the central part of the Cameroon Line (Central Africa)", *Journal of African Earth Sciences*, 147, 20-27, 2018.

[12] Ngounouno, I., Moreau, C., Déruelle, B., Demaiffe, D., Montigny, R., "Pétrologie du complexe alcalin sous-saturé de Kokoumi (Cameroun)", *Bulletin de la Société Géologique de France*, 172, 675-686, 2001.

[13] Njonfang, E., Moreau, C., "The mafic mineralogy of the Pandé massif, Tikar plain, Cameroon: implications for a peralkaline affinity and emplacement from highly evolved alkaline magma", *Mineralogical Magazine*, 64, 525-537, 2000.

[14] Kamdem, J.B, Kraml, M., Keller, J., Henjes-Kunst-F, "Cameroon Line magmatism: conventional K/Ar and single-crystal laser ^{40}Ar/^{39}Ar ages of rocks and minerals from the Hosséré Nigo anorogenic complex, Cameroon", *Journal of African Earth Sciences* 35 (1): 99-105, 2002.

[15] Ngonge, E.D., Hollanda, M.H.B.M., Nsifa Nkonguin, E., Tchoua, M.F., "Petrology of the Guenfalabo ring-complex: An example of complete series along the Cameroon Volcanic Line (CVL), Cameroon", *Journal of African Earth Sciences*, 96, 139-154, 2014.

[16] Itiga, Z., Chakam Tagheu, P.J., Wotchoko, P., Wandji, P., Bardintzeff, J.M., Bellon, H., "La ligne du Cameroun: Volcanologie et géochronologie de trois régions (mont Manengouba, plaine du Noun et Tchabal Gangdaba)", Géochronique, 91, 13-16+ p. 3 couv., 2004.

[17] Itiga, Z., Bardintzeff, J.M., Wotchoko, P., Wandji, P., Bellon, H., "Tchabal Gangdaba massif in the Cameroon Volcanic Line: a bimodal association", *Arabian Journal of Geosciences*, 7, 11: 4641-4664, 2014.

[18] Itiga, Z., Bonin, B., Bardintzeff, J.M., Wandji, P., Ngo Belnoun, R.N., Mbassa, B.J., Wotchoko, P., Tchokona Seuwui, D., Ntepe Nfomou,. Bellon, H., "The Pan-African post-collision Hosséré Mana plutonic complex and associated Gapi Stock (Western Cameroon Domain, Cameroon): Petrology, mineralogy and geochemistry", *Journal of African Earth Sciences*, 149, 398-425, 2019.

[19] Toteu, S.F., Penaye, J., Poudjom Djomani, Y., "Geodynamic evolution of the Pan-African belt in central Africa with special reference to Cameroon", *Canadian Journal of Earth Sciences*, 41, 73-85, 2004.

[20] Bellon, H., Rangin, C., "Geochemistry and isotopic dating of Cenozoic volcanic arc sequences around the Celebes and Sulu Seas", *Proceedings of the Ocean Drilling Program: Scientific Results*, 124, 1991.

[21] Steiger, R.H., Jäger, E., "Subcommission on geochronology: Convention on the use of decay constants in geo-and cosmochronology", *Earth and Planetary Science Letters*, *36*, 356-362, 1977.

[22] Mahood, G.A., Drake, R.E., "K-Ar dating young rhyolitic rocks: a case study of Sierra la Primavera, Mexico", *Geological Society American Bulletin*, 93, 1232-1241, 1982.

[23] Morimoto, N., Fabries, J., Ferguson, A.K., Ginzburg, I.V., Ross, M., Seifert, F.A., Zussman, J., Aoki, K., Gottardi, G., "Nomenclature of pyroxenes", *Mineralogical Magazine*, 52, 535-550, 1988.

[24] Hawthorne, F.C., Oberti, R., Harlow, G.E., Maresch, W.V., Martin, R.F., Schumacher, J.C., Welch, M.D., "Nomenclature of the amphibole supergroup", *American Mineralogist*, 97, 11-12, 2031-2048, 2012.

[25] Le Maitre, R.W. (Ed), "Igneous Rocks, a Classification and glossary of terms. (Recommendations of the International Union of Geological Sciences Subcommission on the Systematics of Igneous Rocks)" *Cambridge University Press, Cambridge, UK*, 2002.

[26] Miyashiro, A., "Nature of alkalic volcanic rocks series", *Contributions to Mineralagy and Petrology*, 66, 91-104, 1978.

[27] Shand, S.J., "Eruptive Rocks. Their Genesis, Composition, Classification, and Their Relations to Ore-deposits", *Wiley, New York*, 444 pp., 1943.

[28] Maniar, P.D., Piccoli, P.M., "Tectonic discrimination of granitoids", *Geological Society and of America Bulletin*, 101, p. 635-643, 1989.

[29] Chappell, B.W., White, A.J.R., "Two contrasting granite types". *Pac. Geol.* 8, 173-174, 1974.

[30] Frost, B.R., Arculus, R.J., Barnes, C.G., Collins, W.J., Ellis, D.J., Frost, C.D., "A geochemical classification of granitic rocks", *Journal of Petrology*, 42, 2033-2048, 2001.

[31] McDonough, W.F., Sun, S.S., "The composition of the Earth", *Chemical Geology*, 120, 223-253, 1995.

[32] Rudnick, R.L., Gao, S., "Composition of the Continental Crust. "Treatise on Geochemistry", *Elsevier (Ed.)*, 3, 1-64, 2003.

[33] Sun, S.S., McDonough, W.F., "Chemical and isotopic systematics of oceanic basalts: implications for mantle composition and processes", *In: Saunders, A.D., Norry, M.J. (Eds.), Magmatism in the Ocean Basins, vol. 42. Geological Society Special Publication*, 313-345, 1989.

[34] Pearce, J.A., Harris, N.J., Tindle, A., "Trace element discrimination diagrams for the geotectonic interpretation of granite rocks", *Journal of Petrology*, 15, 956-983, 1984.

[35] Eby, G.N., "Chemical subdivision of A-type granitoids: petrogenetic and tectonic implications", *Geology*, 20, 641-644, 1992.

[36] Bonin, B., "A-type granites and related rocks: evolution of a concept, problems and prospects", *Lithos*, 97, 1-29, 2007.

[37] Thiéblemont, D., Tegyey, M., "Une discrimination géochimique des roches différenciées témoin de la diversité d'origine et de situation tectonique des magmas calco-alcalins", *Comptes Rendus Acad. Sci. Paris*, Ser. II, 319, 87-94, 1994.

[38] Gorton, M.P., Schandl, E.S., "From continents to island arcs: a geochemicalindex of tectonic setting for arc-related and within-plate felsic to intermediate volcanic rocks", *Canadian Mineralogist*, 38, 1065-1073, 2000.

[39] Schandl, E.S., Gorton, M.P., "Application of high field strength elements to discriminate tectonic settings in VMS environments", *Economic Geology*, 97,629-642, 2002.

[40] Pearce, J.A., "Trace element characteristics of lavas from destructive plate boundaries", *In: Thorpe, R.S. (Ed.), Andesites: Orogenic Andesites and Related Rocks. John Wiley, Chichester*, pp. 525–548, 1982.

[41] Pearce, J.A., "Role of the sub-continental lithosphere in magma genesis at active continental margins", *In: Hawkesworth, C.J., Norry, M.J. (Eds.), Continental Basalts and Mantle Xenoliths. Shiva, Nantwich*, 230-249, 1983.

[42] Coish, R.A., Sinton, C.W, "Geochemistry of mafic dikes in the Adirondac mountains: implications for the constitution of Late Precambrian mantle", *Contributions to Mineralogy and Petrology*, 110, 500-514, 1992.

[43] Green, T.H., "Significance of Nb/Ta as an indicator of geochemical processes in the crust mantle system", *Chemical Geology*, v. 120, 347-359, 1995.

[44] Wang, K., Plank, T., Walker, J.D., Smith, E.I., A mantle melting profile across the Basin and Range, SW USA", *Journal of Geophysical Research*, 107, B1-21, 2002.

[45] Barbarin, B., "A review of relationships between granitoids types, their origins and their geodynamic environments", *Lithos*, 46, 605-626, 1999.

[46] Chappel, B.W., "Aluminium saturation in I- and S-type granites and the characterization of the fractionated haplogranites", *Lithos*, 46, 535-551, 1999.

[47] Mbassa, B.J., Kamgang, P., Grégoire, M., Njonfang, E., Benoit, M., Itiga, Z., Duchene, S., Bessong, M., Wokwenmendam Nguet, P., Ntepe Nfomou, "Evidence of heterogeneous crustal origin for the Pan-African Mbengwi granitoids and the associated mafic intrusions (North western Cameroon, central Africa)", *Comptes Rendus Géoscience*, 348, 116-126, 2016.

[48] Anderson, J.L., Morrison J., "Ilmenite, magnetite and peraluminous Mesoproterozoic anorogenic granites of Laurentia and Baltica", *Lithos*, 80, 45-60, 2005.

[49] Joron, J.L., Cabanis, B., Treuil, M., "Méthodes d'identification des séries anciennes basées sur la géochimie des éléments en

traces", *Centre Recherches Exploration-Production Elf Aquitaine*, 7, 1, 273-284, 1983.

[50] Cox, K.G., Bell, J.D., Pankhurst, R.J., "The interpretation of igneous rocks", *George, Allen and Unwin, London, Boston, Sydney*, 1979.

[51] Daly, R.A., "The geology of Ascension Island", *Proc. Am. Acad. Arts Sci.*, 60, 1-80, 1925.

[52] Watson, E.B., Harrison, T.M., "Zircon saturation revisited: temperature and composition effects in a variety of crustal magma types", *Earth and Planetary Science Letters*, 64 (2), 295-304, 1983.

[53] Harrison, T.M., Watson, E.B., "The behavior of apatite during crustal anatexis: equilibrium and kinetic considerations". *Geochemica Cosmochimica Acta*, 48 (7), 1467-1477, 1984.

[54] Andersen, D.J., Lindsley, D.H., "New and final model for the Ti-magnetite/ilmenite geothermometer and oxygen barometer", *Abstract AGU 1985. Spring meeting Eos. Transaction American Geophysical Union*, 66 (18), 416, 1985.

[55] Lepage, L.D., "ILMAT: an excel worksheet for ilmenite-magnetite geobarometry and geobarometry", *Computers and Geosciences*, 29 (5) 673-678, 2003.